APPLICATIONS OF COUPLED CLUSTER THEORY ON

AL, LI, N, AND O-CONTAINING SMALL MOLECULES

by

JUSTIN MATTHEW TURNEY

(Under the Direction of Henry F. Schaefer, III)

ABSTRACT

Two sets of isomers, dialuminum monoxide (AlOAl / AlAlO) and lithium nitroxide (LiON / LiNO), are investigated with a variety of high-level *ab initio* techniques. The electronic structure of the AlAlO isomer was of particular difficulty due to its weak metal-metal bonding, likewise for its transition state to AlOAl. A detailed study of its ground state potential energy surface was conducted to address the question of why experimentalists have been unable to detect AlAlO.

A different problem has plagued the history of lithium nitroxide. Application of one level of theory suggests LiON to be the energetic minimum. Use of another favors LiNO. Then to complicate the matter even more, there is a possibility of a bent structure as well. A definitive study of this system including their connecting transition states has been performed using coupled cluster theory and sufficiently large basis sets.

INDEX WORDS: *ab initio* quantum chemistry, coupled cluster, multireference configuration interaction, multiconfiguration self consistent field, complete active space self consistent field, dialuminum monoxide, AlOAl, AlAlO, lithium nitroxide, LiON, LiNO, potential energy surface, transition state

APPLICATIONS OF COUPLED CLUSTER THEORY ON AL, LI, N, AND O-CONTAINING SMALL MOLECULES

by

JUSTIN MATTHEW TURNEY

B. Sc., Sam Houston State University, 2002

A Dissertation Submitted to the Graduate Faculty

of The University of Georgia in Partial Fulfillment

of the

Requirements for the Degree

DOCTOR OF PHILOSOPHY

ATHENS, GEORGIA

2006

APPLICATIONS OF COUPLED CLUSTER THEORY ON AL, LI, N, AND O-CONTAINING SMALL MOLECULES

by

JUSTIN MATTHEW TURNEY

Major Professor: Henry F. Schaefer, III

Committee: Nigel A. Adams
Geoffrey D. Smith

Electronic Version Approved:

Maureen Grasso
Dean of the Graduate School
The University of Georgia
May 2006

ACKNOWLEDGEMENTS

It is hard to believe that four years have come and gone here at the CC(Q)C. Of course, this time would not have been enjoyable without the following people either standing at my side or having my back:

Foremost, I must express my gratitude to Professor Schaefer for allowing me the chance to be a member of his research group. His advising style allows for freedom to explore any area of quantum chemistry that is of personal interest. Prof. Schaefer allows for many useful discussions and collaborative opportunities with many of the prominent researchers in our field either through visits or the attending of conferences.

Dr. Yamaguchi deserves a great deal of appreciation for his patience to teach and willingness to help me understand key concepts. Group members should take advantage of his experience in applying *ab initio* theory to a vast array of systems.

Next, the administrative staff of the CC(Q)C must be greatly appreciated: Mrs. Linda Rowe, Mrs. Amy Peterson, and Ms. Karen Branch. Their continuous effort to shield all of us from the bureaucracies of the University is greatly treasured.

I also wish to express gratitude my fellow graduates: Brian, Holly, Joe, Steven, and Veronika. It has been an enjoyable four years with you and I hope to remain in contact with each of you for years to come. Thank you also to my friend Matt Wodrich. Countless talks, lunches, and football games have made the entire process bearable. I

must not forget my officemate, Francesco, who has always provided words of encouragement in our conversations of both chemical and non-chemical origin.

There are of course people I would like to thank that are not associated with the Center or even the group. I would like to thank my family in Christ and specifically the *gNelsis* young adult ministry: Harvey and Karen, David, Jared, and Jessica. These people provided an outlet and source for friendship that is in no way related to work. They are a source of strength for which I am most grateful.

Mrs. Joan Bailes, my high school chemistry teacher, must be acknowledged. She was the one that inspired me to choose chemistry as a major in college and then to continue on into graduate school.

Lastly and most humbly I must thank my parents, Jim and Sally, and sister, Jennifer. Without them, my love for chemistry would not have been cultured and formed into what it has become today.

TABLE OF CONTENTS

Page

LIST OF TABLES

Page

LIST OF FIGURES

Page

CHAPTER 1

INTRODUCTION AND LITERATURE REVIEW

1.1 INTRODUCTION TO ELECTRONIC STRUCTURE THEORY

The summary of electronic structure theory provided herein is by no means complete, and readers are encouraged to seek historical and technical details in numerous review articles and books.[1-8] Manipulation of the time-independent non-relativistic Schrödinger equation using quantum mechanics based solely on fundamental physical constants has largely followed the same formula since Boys initiated the development of configuration interaction (CI) methods.[9] The Schrödinger equation,

$$\hat{\mathcal{H}}\left|\Psi\right\rangle = \varepsilon\left|\Psi\right\rangle \tag{1.1}$$

where

$$\begin{aligned}\hat{\mathcal{H}} = &-\sum_{i=1}^{N}\frac{1}{2}\nabla_i^2 - \sum_{A=1}^{M}\frac{1}{2M_A}\nabla_A^2 - \sum_{i=1}^{N}\sum_{A=1}^{M}\frac{Z_A}{r_{iA}} \\ &+\sum_{i=1}^{N}\sum_{j>i}^{N}\frac{1}{r_{ij}} + \sum_{A=1}^{M}\sum_{B>A}^{M}\frac{Z_A Z_B}{R_{AB}}\end{aligned} \tag{1.2}$$

is an eigenvalue equation dependent on the relative position vectors N electrons (r_{ij}) and M nuclei (R_{AB}) of atomic number Z, as well as the nuclear-electronic distance (r_{iA}).

The Born-Oppenheimer approximation is central to quantum chemistry.[10] Since nuclei are much heavier than electrons, they move more slowly. By assuming the N electrons are traveling in a static nuclear field, the Born-Oppenheimer approximation, or the "clamped nuclei" approximation is applied. Within this approximation, the second term of Eq. 1.2, the kinetic energy of the nuclei, can be neglected and the last term of Eq. 1.2, the repulsion between the nuclei, can be considered to be constant. Any constant added to an operator only adds to the operator eigenvalues and has no effect on the operator eigenfunctions. The terms that remain from Eq. 1.2 are called the electronic Hamiltonian,

$$\hat{\mathcal{H}}_{\text{elec}} = -\sum_{i=1}^{N}\frac{1}{2}\nabla_i^2 - \sum_{i=1}^{N}\sum_{A=1}^{M}\frac{Z_A}{r_{iA}} + \sum_{i=1}^{N}\sum_{j>i}^{N}\frac{1}{r_{ij}} \qquad (1.3)$$

which are the electronic kinetic energy, the Coulombic electron-nuclear attraction, and the electronic repulsion, respectively. A constant accounting for the nuclear repulsion must be added at the end,

$$\sum_{A}^{M}\sum_{B}^{M}\frac{Z_A Z_B}{R_{AB}} \qquad (1.4)$$

As is well-known, only for small and / or highly constrained many-body systems Eq. 1.3 can be solved exactly, due to the mathematical challenge of determining the inter-electronic distance, $\sum_{i}^{N}\sum_{j>i}^{N}\frac{1}{r_{ij}}$.[11-15] From this inability to exactly solve Eq. 1.3, modern quantum chemistry is build upon layers of approximations. Yet even the simplest approximations of the electronic wave function met with encouraging early success when compared to experimentally known results.[6,16-19] Since then the entire field of quantum chemistry has thrived with the goal of systematically and rigorously improving the accuracy and efficiency of these approximations.

For molecular systems, we can take linear combinations of atomic orbitals (functions describing the radial character of one electron in the component atoms) in order to define molecular orbitals (MOs).[20] Taking the Pauli exclusion principle into account, Slater determinants are written as antisymmetrized products of MOs, describing both the spin and spatial distribution on one-electron (χ_a).[6,21,22] In terms of defined finite atomic orbital basis sets for all atoms in the molecular system, one can use chemical intuition to write the Slater determinant as the ground state wave function, resulting in the Hartree-Fock (HF) wave function,

$$\Psi^{HF}(\mathbf{x}_1\mathbf{x}_2\cdots\mathbf{x}_n) = \left|\chi_a(\mathbf{x}_1)\chi_b(\mathbf{x}_2)\cdots\chi_z(\mathbf{x}_n)\right\rangle. \qquad (1.5)$$

The wave function of Eq. 1.5 is computed by diagonalizing the matrix of the HF antisymmetrized MO products,

$$\Psi^{HF} = (N!)^{-1/2}\begin{vmatrix} \chi_a(\mathbf{x}_1) & \chi_b(\mathbf{x}_1) & \cdots & \chi_N(\mathbf{x}_1) \\ \chi_a(\mathbf{x}_2) & \chi_b(\mathbf{x}_2) & & \chi_N(\mathbf{x}_2) \\ \vdots & & \ddots & \vdots \\ \chi_a(\mathbf{x}_N) & \chi_b(\mathbf{x}_N) & \cdots & \chi_N(\mathbf{x}_N) \end{vmatrix} \qquad (1.6)$$

The eigenvectors of this matrix can be optimized with the iterative self-consistent field (SCF) method.[18,23] and then operated upon to obtain expectation values for the electronic energy and observable physical quantities of the system at a specified nuclear geometry. Solution of the optimal MO set follows the variational principle,

$$\left\langle \Psi^{HF} \middle| \hat{H} \middle| \Psi^{HF} \right\rangle \le \varepsilon_0 \qquad (1.7)$$

where the expectation value of the Hamiltonian operating on the HF wave function is an upper bound to the exact electronic energy of the system.

In order to optimize the MOs, they must be represented in a form that can be parameterized. The most computationally elegant depiction of MOs is obtained by expansion of contracted Gaussian-type atomic orbitals (CGTOs).[24,25] The use of a finite CGTO basis set implies that the SCF solution to the wave function is only an approximation of the true infinite basis (also called the "complete basis set") HF wave function.

The MO is the most fundamental quantity in contemporary quantum chemistry. Almost all of our understanding of "what the electrons are doing in molecules" is based on the molecular orbital concept. Also most of the computational methods used today start by a calculation of the MOs of the system.

1.2 ELECTRON CORRELATION

By employing the HF approximation, the Schrödinger equation is treated as a one-body problem and a vast simplification is built into the electronic structure problem. Of course, the electronic wave function is actually dependent on the motion of all *N*-electrons, and the many-body interactions of all electrons within the system must be included. Though HF theory can essentially recover 95 – 99% of the total energy for a given atomic or molecular system, it is on the scale of the unaccounted energy that chemically significant phenomena such as bonding, vibrational and rotational interactions, molecular isomerization, and electronic excitations occur. In the 1950s, deficiencies of the HF method were already well known and it became prudent to employ a linear combination of a larger set of Slater determinants, inclusive of the HF Slater determinant, and to optimize their relative contributions to the electronic wave function.

Generally termed configuration interaction (CI),[9,24,26] is was proven that if the coefficients of the entire set of Slater determinants were determined, then the time independent, non-relativistic electronic wave function would be exactly solved within the constraints of the chosen finite basis set. Inclusion of all Slater determinants gives what is called the "full CI" wave function. Löwdin[17] first defined the correlation energy as the difference between the full CI energy expectation value and the HF energy expectation value,

$$\varepsilon_{corr} = \varepsilon_{full\ CI} - \varepsilon_{HF}\,. \tag{1.8}$$

For *N* electrons, and *2K* spin orbitals (basis functions), the number of possible Slater determinants and thus the size of the CI matrix can be determined by,

$$\frac{(2K)!}{N!(2K-N)!}, \tag{1.9}$$

which is computationally feasible for a small (but growing) number of systems. Truncating the full CI wave function and optimizing a smaller set of the most "important" Slater determinants remains the best trade-off computational tractability and wave function accuracy.

Correlated *ab initio* methods employing a trial molecular wave function are generally divided into three major categories: (1) a many-body perturbation correction to the HF wave function, (2) CI expansions (also including multi-configuration self-consistent field methods) where a linear excitation operator is applied to generate a range of possible substitutions from the occupied MOs of the HF reference into the unoccupied orbital space,

$$\left|\Psi_{CI}\right\rangle = c_0\left|\Psi_{HF}\right\rangle + \sum_{r,a} c_a^r \left|\Psi_a^r\right\rangle + \sum_{\substack{a<b \\ r<s}} c_{ab}^{rs}\left|\Psi_{ab}^{rs}\right\rangle + \cdots, \qquad (1.10)$$

and (3) coupled cluster (CC) expansions where the products of substituted determinants are incorporated in the exponential "cluster" excitation operators in order to approximate the effects of higher-order substitutions,

$$\Phi_{CC} \equiv e^{\hat{T}}\Psi_{HF} \qquad (1.11)$$

$$e^{\hat{T}} = 1 + \hat{T} + \frac{\hat{T}^2}{2!} + \frac{\hat{T}^3}{3!} + \cdots. \qquad (1.12)$$

A consequence of truncating the CI / CC expansion of the electronic wave function is that two different types of electron correlation emerge. One type is the short-range interaction of electrons in a system, often called the "instantaneous interaction". The antisymmetric nature of the HF wave function subtly accounts for some of this short-range interaction because of the Pauli exclusion principle, as the wave function will become zero (called a "Fermi hole") when two electrons with equivalent spin occupy the

same spatial coordinates. However, the positions of electrons with opposite spin do not depend on each other. The instantaneous Coulombic repulsion of electrons with opposite spin can be grossly underestimated. If electrons are allowed to "jump" into unoccupied MOs of higher energy, there is a small, but finite chance that *N*-electrons can occupy the same region of space. By allowing occupation of these MOs (previously unoccupied in the HF approximation) some percentage of this new Slater determinant will contribute to the correlated wave function. It is expected that the kinetic energy of the system will get higher and the potential energy of the system will lower dramatically when two electrons are about to "collide". It is the Virial Theorem that dictates an overall lowering of the electronic energy when considering electron correlation, as the electronic potential energy is proportional to double the kinetic energy,

$$-T(\chi) = V(\chi). \qquad (1.13)$$

To summarize, inclusion of excited determinants (configurations) and the instantaneous interaction of electrons within them describes the electron dynamic. Our terminology is combined to conclude that the configuration interaction is solved for in order to recover the "dynamical correlation" of electrons in the system.

Sinanoğlu[27] first proposed the second type of electron correlation, when multiple Slater determinants strongly contribute to the wave function, sometimes approaching or containing degeneracy with the zeroth-order HF approximation. This can occur in situations when someone is trying to characterize bond-breaking, geometries near transition-states, molecules containing atoms with near-degenerate atomic orbitals, or excited electronic states. This effect is known as long-range correlation, often called

"non-dynamical" or "static" correlation. Atoms or molecules containing significant non-dynamical correlation are often referred to as "multireference" systems.

The belief that SCF can yield sufficient accuracy, though it can be justified in some system, can be very wrong in others. That SCF can lead to meaningless chemical prediction was dramatically established by calculations on the F_2 molecule.[28] These calculations reported a negative binding energy for F_2 as large in magnitude as the actual value of 1.6 eV. One can have qualitatively incorrect results with the SCF wave function.

1.3 THE COUPLED CLUSTER HEIRARCHEY

In spite of coupled cluster theory's present utility and popularity, the quantum chemical community was slow to accept it. This is likely due to the unfamiliar mathematical tools that were initially used by the earliest researchers such as Feynman-like diagrams and second-quantization to derive working equations.[29-31] Nearly 10 years after the work of Paldus and Čížek, Hurley presented a re-derivation of the coupled cluster doubles (CCD) equations in terms which were more familiar with quantum chemists.[32] Once the work of Hurley was available the development of coupled cluster experienced a tremendous growth.

Pople[33] and Bartlett[34] were the first to provide computer implementations of CCD that could compute energies for a realistic molecular system. A few years later, Purvis and Bartlett derived and implemented coupled cluster singles and doubles (CCSD) equations.[35] Development continued on to include the construction of highly efficient CCSD energy codes,[35-41] inclusion of higher excitations in the coupled cluster wave function,[42-48] as well as development in analytic first[49-53] and second energy

derivatives.[54-56] For a more in depth overview of coupled cluster's history and a representative derivation of CCSD refer to the review article by Crawford and Schaefer.[1]

In coupled cluster theory, the wave function is parameterized using the following exponential *ansatz*,

$$|\Psi\rangle = e^{T}|0\rangle \tag{1.14}$$

with $|0\rangle$ referring to a single Slater determinant and T being the cluster operator,

$$T = T_1 + T_2 + T_3 + \cdots \tag{1.15}$$

$$T_1 = \sum_i \sum_a t_i^a a^+ i \tag{1.16}$$

$$T_2 = \frac{1}{4} \sum_{ij} \sum_{ab} t_{ij}^{ab} a^+ i b^+ j \tag{1.17}$$

$$T_3 = \frac{1}{36} \sum_{ijk} \sum_{abc} t_{ijk}^{abc} a^+ i b^+ j c^+ k \tag{1.18}$$

where the indices i, j, k, … denote occupied spin orbitals, indices a, b, c, … virtual spin orbitals, and indices p, q, r, … generic orbitals that can be either occupied or virtual. Second-quantized creation and annihilation operators a^+, b^+, i, j, … are used to describe excitations, while t_i^a, t_{ij}^{ab}, … are the actual parameters that need to be determined. The necessary equations can be obtained by first pre-multiplying the Schrödinger equation by e^{-T} and then projecting it onto the reference determinant and on all determinants in the excitation manifold,

$$E = \langle 0|e^{-T} H e^{T}|0\rangle \tag{1.19}$$

$$0 = \langle \Phi_p |e^{-T} H e^{T}|0\rangle \tag{1.20}$$

With the Hamiltonian being defined in the following second-quantized form,

$$\begin{aligned} H &= E_{\mathrm{HF}} + f_N + W_N \\ &= E_{\mathrm{HF}} + \sum_{p,q} f_{pq}\left\{p^+q\right\} + \frac{1}{4}\sum_{p,q,r,s}\langle pq\|rs\rangle\left\{p^+q^+sr\right\} \end{aligned} \tag{1.21}$$

with E_{HF} the Hartree-Fock energy, f_{pq} the Fock matrix elements, and $\langle pq\|rs\rangle$ the antisymmetrized two-electron integrals, we can obtain the explicit expressions for Eqs. 1.19 and 1.20. For the CCSDT model[47,57,58] in which the cluster operator is truncated at triple excitations, these expressions for Eqs. 1.19 and 1.20 become,

$$\Delta E = \langle 0|\left[f_N + W_n\left(T_2 + \frac{1}{2!}T_1^2\right)\right]_c|0\rangle \tag{1.22}$$

$$\begin{aligned} 0 = \langle S|\Big[& f_N T_1 + f_N\left(T_2 + \frac{1}{2!}T_1^2\right) + W_N T_1 \\ & + W_N\left(T_2 + \frac{1}{2!}T_1^2\right) + W_N\left(T_3 + T_1T_2 + \frac{1}{3!}T_1^3\right)\Big]_c|0\rangle \end{aligned} \tag{1.23}$$

$$\begin{aligned} 0 = \langle \mathcal{D}|\Big[& f_N T_2 + f_N\left(T_3 + T_2T_1\right) + W_N + W_N T_1 \\ & + W_N\left(T_2 + \frac{1}{2!}T_1^2\right) + W_N\left(T_3 + T_1T_2 + \frac{1}{3!}T_1^3\right) \\ & + W_N\left(T_3T_1 + \frac{1}{2!}T_2^2 + \frac{1}{2!}T_2T_1^2 + \frac{1}{4!}T_1^4\right)\Big]_c|0\rangle \end{aligned} \tag{1.24}$$

$$\begin{aligned} 0 = \langle \mathcal{T}|\Big[& f_N T_3 + f_N\left(T_3T_1 + \frac{1}{2!}T_2^2\right) + W_N T_2 \\ & + W_N\left(T_3 + T_1T_2\right) + W_N\left(\frac{1}{2!}T_2^2 + T_3T_1 + \frac{1}{2!}T_2T_1^2\right) \\ & W_N\left(T_3T_1 + \frac{1}{2!}T_2^2T_1 + \frac{1}{2!}T_3T_1^2 + \frac{1}{3!}T_2T_1^3\right)\Big]_c|0\rangle \end{aligned} \tag{1.25}$$

where the subscript c means that only connected terms are considered. The symbols S, $\mathcal{D}$, and $\mathcal{T}$ denote in the above equations singly, doubly, and triply excited determinants,

respectively. CCSDT scales as $\mathcal{O}(n^8)$ with n being the size of the system. These other methods attempt to obtain CCSDT *quality* at a lower cost.

Since the cost of performing a CCSDT computation is so high, numerous approximations have been developed in attempts to recover triples excitations at lower cost. One of these approximation models is the CCSDT-*n* series. The first one to be considered is CCSDT-1, this method is also denoted as CCSDT-1a at times.[48] In this method the singles and doubles equations (Eqs. 1.23 and 1.24) are the same as in CCSDT, except that the $W_N T_1 T_3$ term in the doubles is omitted. For the triples only the $f_N T_3$ and $W_N T_2$ terms are included. This yields for CCSDT-1 the following equations,

$$\begin{aligned} 0 = \langle S \| \Big[& f_N T_1 + f_N \left(T_2 + \frac{1}{2!} T_1^2 \right) + W_N T_1 \\ & + W_N \left(T_2 + \frac{1}{2!} T_1^2 \right) + W_N \left(T_3 + T_1 T_2 + \frac{1}{3!} T_1^3 \right) \Big]_c | 0 \rangle \end{aligned} \tag{1.26}$$

$$\begin{aligned} 0 = \langle \mathcal{D} \| \Big[& f_N T_2 + f_N \left(T_3 + T_2 T_1 \right) + W_N + W_N T_1 \\ & + W_N \left(T_2 + \frac{1}{2!} T_1^2 \right) + W_N \left(T_3 + T_1 T_2 + \frac{1}{3!} T_1^3 \right) \\ & + W_N \left(\frac{1}{2!} T_2^2 + \frac{1}{2!} T_2 T_1^2 + \frac{1}{4!} T_1^4 \right) \Big]_c | 0 \rangle \end{aligned} \tag{1.27}$$

$$0 = \langle \mathcal{T} \| \left[f_N T_3 + W_N T_2 \right]_c | 0 \rangle . \tag{1.28}$$

In the CCSDT-1b model the $W_N T_1 T_3$ term removed from the doubles equation of CCSDT-1a is included giving CCSDT's doubles equation. For CCSDT-2, the $W_N T_2^2$ term is included in the triples equations. Singles (Eq. 1.22) and doubles (Eq. 1.23) are the same as CCSDT, the triples equation becomes,

$$0 = \langle \mathcal{T} \| \left[f_N T_3 + W_N T_2 + W_N T_2^2 \right]_c | 0 \rangle \tag{1.29}$$

The final CCSDT-*n* model to be considered is CCSDT-3. This model is considerably more complex than the three models already mentioned. CCSDT-3 includes all terms in the triples equation (Eq. 1.24) except those that explicitly depend on the T_3 amplitudes except the computationally straightforward $f_N T_3$ term. This yields the following triples equation,

$$\begin{aligned} 0 = \left\langle \mathcal{T} \right| \Bigg[& f_N T_3 + \frac{1}{2!} f_N T_2^2 + W_N T_2 \\ & + W_N T_1 T_2 + W_N \left(\frac{1}{2!} T_2^2 + \frac{1}{2!} T_2 T_1^2 \right) \\ & W_N \left(\frac{1}{2!} T_2^2 T_1 + \frac{1}{3!} T_2 T_1^3 \right) \Bigg]_c \left| 0 \right\rangle \end{aligned} \tag{1.30}$$

Another CCSDT approximation that should be considered is the CC3 model.[59] The CC3 model has been designed for the calculation of dynamical properties and excitation energies. In comparison with the CCSDT-*n* models it is similar to CCSDT-1 in that only the lowest-order contributions to the triples equations are retained. In CC3 single excitations are treated as zeroth-order to account for orbital relaxations, while CCSDT-*n* is based on usual perturbation theory in which T_2 and T_1 are treated as first- and second-order contributions, respectively. For CC3 the singles, doubles, and triples equations omit all terms that include a T_1 contribution.

1.4 MULTICONFIGURATION SELF-CONSISTENT FIELD THEORY

The multiconfiguration self-consistent field theory (MCSCF), which consists of optimizing both the mixing of several configurations as well as the orbitals of which they are composed, would appear to be a natural extension of the one-configuration HF method. Early on MCSCF did not receive a great deal of attention due notably two main

reasons: 1) SCF wave function was thought to be "sufficiently" accurate for most of the interesting properties of a chemical system; and 2) the successful implementation of the single configuration SCF method was difficult and the implementation of the more complex MCSCF framework proved to be significantly more demanding.[60]

The concept of the MO is not restricted to the HF model described above. Sets of orbitals can be constructed for more complex wave functions, which include correlation effects this is the idea of multiconfigurational self-consistent field theory (MCSCF). They can be used to obtain insight into the detailed features of the electronic structure. One choice of orbitals are the natural orbitals, which are obtained by diagonalizing the spinless first-order reduced density matrix. The occupation numbers (η) of the natural orbitals are not restricted to 2, 1, or 0, as in the HF MOs. Instead they fulfill the condition,

$$0 < \eta < 2. \qquad (1.31)$$

If the HF determinate dominates the wave function, some of the occupation numbers will be close to 2 and the corresponding MOs will closely resemble the canonical HF MOs. The remaining natural orbitals will have small occupation numbers, which can be considered as different types of correlation effects in the molecule.

Configuration-mixing or configuration interaction (CI) as it is popularly called can be very important in atomic spectroscopy, electron-atom scattering, and other atomic phenomena. van der Waals interaction, i.e., the attractive long-range interaction of two systems, can not be explained without going beyond SCF. Generally speaking, the SCF wave function can only be regarded as a starting point for more accurate calculation and should be used very cautiously in making predictions on the chemical behavior of a

system. Refer to Fig. 1.1 for a pictorial example of SCF inadequacies compared to MCSCF and FCI.

1.4.1 Illustrative Example of a MCSCF Wave Function

To help in the understanding of the need for a multiconfiguration wave function an illustrative example is very insightful. Let us consider the dissociation of a single bond; the hydrogen molecule, H_2. The MOs for this molecule can be written in the form,

$$\varphi_i = \mathrm{N}_i(\chi_{iA} \pm \chi_{iB}) \tag{1.32}$$

where χ_{iA} and χ_{iB} are two functions located at the two nuclei, with the property,

$$\hat{i}\chi_{iA} = \chi_{iB} \tag{1.33}$$

where $\hat{i}$ is the inversion operator. N_i is the normalization constant. For H_2, the ground state wave function is at the equilibrium geometry dominated by the electronic configuration $(\varphi_1)^2$, where the molecular orbital φ_1 is doubly occupied. φ_1 is a bonding orbital built from two atomic orbitals χ_{iA} and χ_{iB} with their main contribution from the hydrogen 1*s* orbital: $\chi_{iA} = 1s_A + "small\ corrections"$.

The "*small corrections*" are important in a quantitative description of the H_2 chemical bond, but for the present qualitative illustration it can be neglected and then write,

$$\varphi_1 = \mathrm{N}_1(1s_A + 1s_B)\,. \tag{1.34}$$

This MO is in the restricted Hartree-Fock (RHF) model assumed to be doubly occupied leading to a total wave function of the form,

$$\Phi_1 = \varphi_1(\mathbf{r}_1)\varphi_1(\mathbf{r}_2)\Theta_{2,0} \tag{1.35}$$

which will be simply denoted as $(\varphi_1)^2$. $\Theta_{2,0}$ is the singlet (S=0) spin function for two electrons,

$$\Theta_{2,0} = \sqrt{\tfrac{1}{2}}\left(\alpha_1\beta_2 - \beta_1\alpha_2\right) \tag{1.36}$$

The RHF models leads to a reasonable accurate for H_2 near the equilibrium geometry: computed bond distance is 0.7337 Å with the cc-pVQZ basis set (experimental[61] 0.74144 Å) and a bond energy of 83.8 kcal mol^{-1} (experimental[61] 103.3 kcal mol^{-1}). It has been shown many times that the RHF model is capable of describing a closed shell system around its equilibrium geometry rather well. The correlation energy is only a small fraction of the total energy, but it is strongly distance dependent, which explains the error in the computed bond energy. There is no correlation energy at all for two separated hydrogen atoms.

Expanding the wave function as products of the atomic orbitals $1s_A$ and $1s_B$:

$$\begin{aligned}\Phi_1 = \mathrm{N}_1^2\big[&1s_A(\mathbf{r}_1)1s_A(\mathbf{r}_2) + 1s_A(\mathbf{r}_1)1s_B(\mathbf{r}_2)\\ &+1s_B(\mathbf{r}_1)1s_A(\mathbf{r}_2) + 1s_B(\mathbf{r}_1)1s_B(\mathbf{r}_2)\big]\Theta_{2,0}\end{aligned} \tag{1.36}$$

You will notice that this wave function contains terms where both electrons are on the same atom. At larger bond separations these terms are unphysical since they correspond to dissociation into $H^+ + H^-$, which is much higher in energy. This leaves only the middle two terms that correctly describe the dissociated products.

For the RHF model it is a typical feature to include these “ionic structures” in fixed proportions into the wave function. As a consequence the model cannot be used to describe dissociation processes resulting in products with open shells. This is seen in Fig. 1.1 with the SCF curve much higher above the true energy at the separated limit.

The most straightforward method to solve this problem is to introduce coefficients in front of the different terms in the wave function above,

$$\Psi = C_{\text{ion}}\Phi_{\text{ion}} + C_{\text{cov}}\Phi_{\text{cov}} \tag{1.37}$$

where

$$\Phi_{\text{ion}} = \text{N}_{\text{ion}}\left[1s_A(\mathbf{r}_1)1s_A(\mathbf{r}_2) + 1s_B(\mathbf{r}_1)1s_B(\mathbf{r}_2)\right]\Theta_{2,0} \tag{1.38}$$

$$\Phi_{\text{cov}} = \text{N}_{\text{cov}}\left[1s_A(\mathbf{r}_1)1s_B(\mathbf{r}_2) + 1s_B(\mathbf{r}_1)1s_A(\mathbf{r}_2)\right]\Theta_{2,0} \tag{1.39}$$

In these equations the C coefficients can be varied to yield the correct wave function at the separated limit ($C_{\text{ion}} = 0$). At the equilibrium geometry $C_{\text{ion}} \approx C_{\text{cov}}$ which reflects the fact that the RHF determinate dominates the wave function. The wave function given above is only for the bonding wave function; in order to have a non-orthogonal basis the anti-bonding orbitals must be included,

$$\varphi_2 = \text{N}_2(1s_A - 1s_B). \tag{1.40}$$

In terms of φ_1 and φ_2 the wave function of Eq. 1.37 becomes

$$\Psi = C_1\Phi_1 + C_2\Phi_2 \tag{1.41}$$

where Φ_2 is the electronic configuration $(\varphi_2)^2$. This is the multiconfigurational MO formulation of the wave function for the chemical bond in H_2. This wave function will correctly describe the entire potential energy surface. Near equilibrium $C_1 \sim 1$ and $C_2 \sim 0$, while at large separations $C_1 \sim -C_2$. This description of the wave function includes the description of the chemical bond in terms of bonding and anti-bonding orbitals.

This simple case illustrates the need of a multiconfiguration method for describing molecular systems. Other areas that this method is needed in is the dissociation of several bonds simultaneously, molecules with competing resonance structures, and in some transition states on the energy surface.

It should be noted that the number of configuration state functions (CSFs) will increase very quickly with the number of *active* orbitals. In most cases one does not worry about the exact construction of the MCSCF wave function that leads to the correct dissociation. Simply use all the CSFs that can be constructed by distributing the electrons among the active orbitals. This is the idea behind the Complete Active Space SCF (CASSCF) method.

Complete derivation of MCSCF will not be included here the reader is encouraged to seek other references for a more complete description of the derivation.[60]

1.5 SYSTEMS OF INTEREST

The first system that will be discussed is that of dialuminum monoxide. This molecule has led an interesting life through the inconsistencies in the determination of its structural geometry. Its structure went back and forth several times from being a bent to a linear geometry, before finally deciding on a linear one. While the symmetric AlOAl has been studied experimentally and some by theory, no definitive work was conducted on the AlAlO isomer. Experimentalists seemed unable to observe this asymmetric isomer. Inspection of both isomers and the transition state connecting them was done to determine the reason for the absence of AlAlO in experiments. Results and analyses are presented in Chapter 2.

The second system that is of interest is lithium nitroxide. Inconsistencies between various levels of theory, as well as basis sets, exist as to the minimum energy isomer. The linear LiON and LiNO isomers are nearly degenerate in their energies and is the source of the discrepancy between methods. Both isomers and the transition state that connects

them were studied using coupled cluster theory and basis sets up to quadruple-*zeta* in quality. Due to the ionic nature of the system core effects for lithium were also included by using basis sets specifically designed to handle core electrons. The results of this study are presented in Chapter 3.

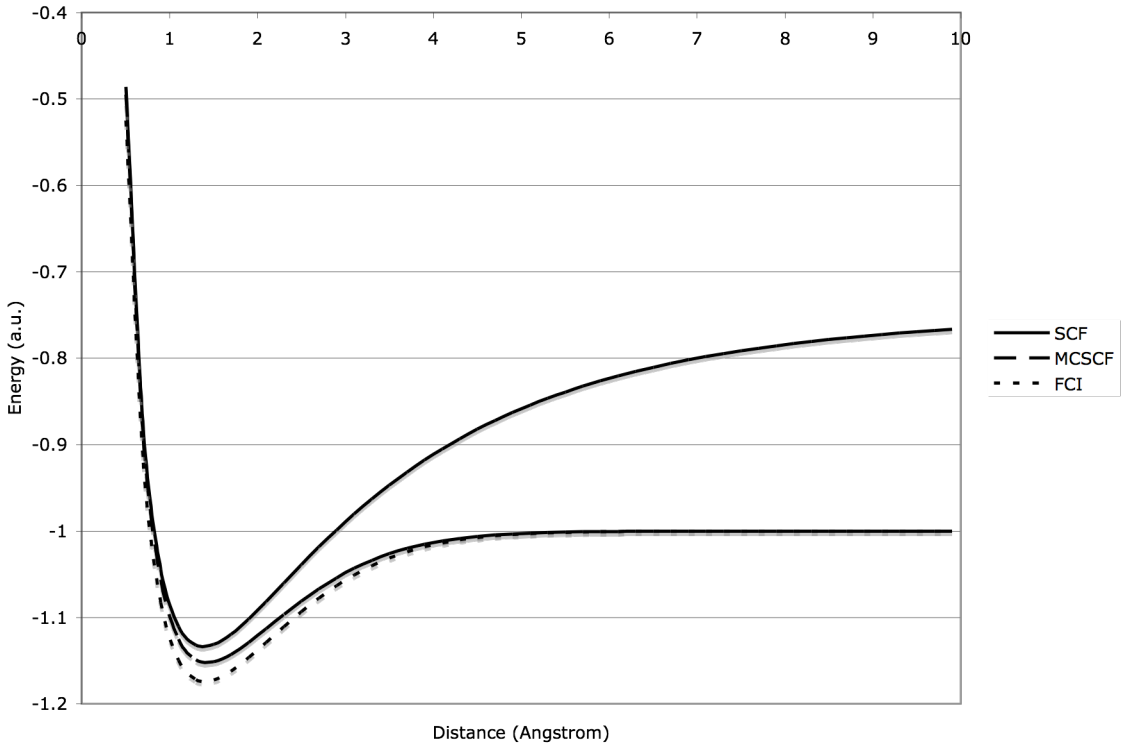

Figure 1.1: Potential energy curves for H_2 showing the erratic behavior of SCF as a function of the internuclear distance. For comparison the MCSCF and FCI curves are given which dissociate correctly.

CHAPTER 2

THE SINGLET ELECTRONIC GROUND STATE ISOMERS OF DIALUMINUM MONOXIDE: AlOAl, AlAlO, AND THE TRANSITION STATE CONNECTING THEM[†]

[†] Justin M. Turney, Levent Sari, Yukio Yamaguchi, and Henry F. Schaefer, III, *J. Chem. Phys.* **122**, 094304 (2005).

2.1 ABSTRACT

The singlet electronic ground state isomers, $\tilde{X}\ ^1\Sigma_g^+$ (AlOAl $D_{\infty h}$) and $\tilde{X}\ ^1\Sigma^+$ (AlAlO $C_{\infty v}$) of dialuminum monoxide have been systematically investigated using *ab initio* electronic structure theory. The equilibrium structures and physical properties for the two molecules have been predicted employing self-consistent field (SCF), configuration interaction with single and double excitations (CISD), multireference CISD (MRCISD), coupled cluster with single and double excitations (CCSD), CCSD with perturbative triples [CCSD(T)], CCSD with iterative partial triple excitations (CCSDT-3 and CC3), and full triples (CCSDT) coupled cluster methods. Four correlation consistent polarized valence (cc-pVXZ) type basis sets were used. The AlAlO system is rather challenging theoretically. The two isomers are confirmed to have linear structures at all levels of theory. The symmetric isomer AlOAl is predicted to lie 81.9 kcal mol^{-1} below the asymmetric isomer AlAlO at the cc-pV(Q+d)Z CCSD(T) level of theory. The predicted harmonic vibrational frequencies for the $\tilde{X}\ ^1\Sigma_g^+$ AlOAl molecule, ω_1=517 cm^{-1}, ω_2=95 cm^{-1}, and ω_3=1014 cm^{-1}, are in good agreement with experimental values. The harmonic vibrational frequencies for the $\tilde{X}\ ^1\Sigma^+$ AlAlO structure, ω_1=1014 cm^{-1}, ω_2=73 cm^{-1}, and ω_3=253 cm^{-1}, presently no experimental values with which to be compared. With the same methods the barrier heights for the isomerization AlOAl→AlAlO and AlAlO→AlOAl reaction were predicted to be 84.3 and 2.4 kcal mol^{-1}, respectively. The dissociation energies D_0 for AlOAl ($\tilde{X}\ ^1\Sigma_g^+$) and AlAlO ($\tilde{X}\ ^1\Sigma^+$)→AlO($X\ ^2\Sigma^+$)+Al(^{2}P) were determined to be 130.8 and 48.9 kcal mol^{-1}, respectively. Thus, both symmetric AlOAl ($\tilde{X}\ ^1\Sigma_g^+$) and asymmetric AlAlO ($\tilde{X}\ ^1\Sigma^+$) isomers are expected to be thermodynamically stable with respect to the

dissociation into AlO($X\ ^2\Sigma^+$)+Al(^2P) and kinetically stable for the isomerization reaction AlAlO→AlOAl at sufficiently low temperatures.

2.2 INTRODUCTION

Dialuminum monoxide, specifically symmetric AlOAl, has been the subject of a number of important experimental studies over the past four decades. Prior to any experimental evidence it was assumed that AlOAl had a bent structure of C_{2v} symmetry.[62] Interpretation of the experimental results led to several conflicting conclusions about the equilibrium geometry of AlOAl. Klemperer's early (1963) interpretations of electron deflection experiments[63] suggested that AlOAl has a linear $D_{\infty h}$ geometry. However, infrared (IR) studies published in 1964 based on matrix isolation experiments[64] concluded that AlOAl was bent with an apex angle near 145° and a ν_2 bending mode frequency of 250 cm^{-1}.

The 1970 work of Snelson[65] reported an IR study on matrix isolated AlOAl. This investigation provided fundamental vibrational frequencies for the symmetric [$\nu_1(A_1)$] and antisymmetric [$\nu_3(B_1)$] stretching modes in agreement with previously performed matrix isolation experiments. However, they were unable to observer the bending mode ν_2 of AlOAl down to 190 cm^{-1}. Through comparison with Li_2O, Snelson predicted the ν_2 of AlOAl to occur near 120 cm^{-1}. The following year, Makowiecki, Lynch, and Carlson[66] studied the three fundamental vibrational modes of AlOAl in rare gas matrices. They reported frequencies for the ν_2 mode as 503 cm^{-1} in Ar and 499 cm^{-1} in Kr, but these values lay more than 300 cm^{-1} above previous estimates. This high bending frequency ν_2 suggests the occurrence of a metal-metal bond on AlOAl resulting from a ring-type

structure. Makowiecki described several observations in favor of this interpretation. First, atomization energies for AlOAl are not in sufficient agreement with bond energy calculations for systems containing a metal-metal dissociation also including two metal-oxygen dissociations. Second, electron impact fragmentation of AlOAl in mass spectrometric studies have not given appreciable concentration of the metal dimmer ion Al_2^+ but generate larger concentrations of AlO^+. Third, the ν_2 bending frequencies are only slightly higher than reasonable estimated values for stretching frequencies of the homonuclear Group IIIA metal diatom molecules.

As previously stated, the high ν_2 value could arise from the occurrence of metal-metal bonding giving a ring-type structure. In 1973, Marino and White[67] reported no evidence for even a very weak feature in the 500 cm^{-1} vicinity, where ν_2 had been observed by Makowiecki, until molecular oxygen was introduced into the argon system. In 1974, Lynch, Zehe, and Carlson[68] reported that the ν_2 mode of AlOAl in the vicinity of 500 cm^{-1} is observed only in very concentrated matrices, on the order of 40 μmol and therefore is also likely to be due to an aggregate species. The 1982 Kr matrix study conducted by Douglas, Hauge, and Margrave[69] established the previous unobserved frequency for the ν_1 mode of AlOAl to be 471 cm^{-1}. Using their observed frequency and the work of Marino and White,[67] who were looking for a band assignable to the bend mode frequency, Margrave's group deduced that the ν_1 mode is infrared inactive in accordance with a linear $D_{\infty h}$ structure.

Among more recent experimental studies, the work of Andrews (1992)[70] and of Miller and Bondybey (1991)[71] stands out. A strong IR band detected at 992 cm^{-1} (in Ar matrices[64,66,68,70,72] and in the gas phase[71]) is now attributed to the antisymmetric stretch

vibration ν_3 of the linear AlOAl species. Using Raman spectroscopic techniques the symmetric stretch vibrational frequency ν_1 has been additionally reported at 472 cm^{-1} [in argon (Refs. 73 and 74)] and 525 cm^{-1} (in the gas phase[71]). The bending frequency ν_2 was deduced from experiment to be 99 cm^{-1} by Cai, Carter, Miller, and Bondybey.[71]

A semiempirical theoretical study[75] using complete neglect of differential overlap (CNDO) predicted incorrectly an acute angle structure for AlOAl. Another semiempirical study[76] using modified neglect of diatomic overlap (MNDO) found the heat of formation for Al_2O to be -72 kcal mol^{-1}, which is qualitatively inconsistent with the experimental value of -32 ± 3 kcal mol^{-1}.[77]

According to Pauling's ideas,[78] the electronegativities of Al (χ_{Al} = 1.5) and O (χ_O = 3.5) suggest a partial ionic character of 64%. The work of Masip *et al.*[79] included a Mulliken population analysis of AlOAl. This analysis showed a large charge transfer from the Al atom to the O atom (≈0.9*e*), which indicates a rather ionic molecule.

On the other hand *ab initio* theoretical studies on the asymmetric AlAlO isomer predict a linear geometry that lies 94 kcal mol^{-1} above the AlOAl isomer at the Hartree-Fock (HF)/6-31G* level by Boldyrev and Schleyer[80] and about 80 kcal mol^{-1} at the Møller-Plesset second order perturbation theory (MP2)/6-31G* level by Nemukhim and Weinhold.[81] Additionally, the work of Boldyrev and Schleyer on both the singlet ground states of the AlAlO and AlOAl isomers found the following: for AlAlO ($C_{\infty v}$) r_{AlAl}=2.806 Å and r_{AlO}=1.583 Å at the HF/6-31G* level and for AlOAl ($D_{\infty h}$) r_{AlO}=1.703 Å at the HF/6-31G* level and r_{AlO}=1.733 Å at the MP2(full)/6-31G* level.[80] Their study included the lowest triplet states of the two isomers but they were found to be high in energy and lead to bent (C_{2v}) geometries due to the Renner-Teller effect. Boldyrev and Schleyer also

reported that the asymmetric AlAlO isomer is thermodynamically stable with respect to the dissociation into AlO+Al and may be detectable in matrix isolation experiments, but they did not report the dissociation energy. Currently, no experimental evidence has been found to support this possibility. Nemukhin and Weinhold's theoretical study[81] of aluminum oxides include results for symmetric AlOAl and asymmetric AlAlO. Their findings are as follows: for AlOAl ($D_{\infty h}$) r_{AlO}=1.703 Å restricted Hartree-Fock (RHF/6-31G*) and 1.733 Å (MP2/6-31G*) and for AlAlO ($C_{\infty v}$) r_{AlAl}=2.759 Å, and r_{AlO}=1.648 Å, both at the MP2/6-31G* level. Most recently, Koput and Gertych[82] have reported a coupled cluster [CCSD(T)] study of the vibration-rotation energy levels of the AlOAl global minimum. They predicted fundamental vibrational frequencies within 5 cm^{-1} of the experiments of Cai, Carter, Miller, and Bondybey.[71]

In the present study the singlet electronic ground states of the symmetric ($\tilde{X}\ ^1\Sigma_g^+$ AlOAl) and the asymmetric ($\tilde{X}\ ^1\Sigma^+$ AlAlO) isomers of dialuminum monoxide have been symmetrically studied using the highly correlated wave functions available in our laboratory. Special emphasis is placed on the accurate determination of the relative energy, the barrier heights for the isomerization reaction (AlOAl↔AlAlO), and dissociation energies for the two isomers (AlOAl/AlAlO→AlO+Al) with high levels of theory up to single, double, and iterative partial triple excitations coupled cluster CCSDT-3 (Ref. 46) and CC3 (Ref. 59) methods.

2.3 THEORETICAL PROCEDURES

Four basis sets were employed in order to optimize structures and determine physical properties of AlOAl and AlAlO as well as diatomic AlO. The four basis sets were correlation consistent polarized valence basis sets developed by Dunning and co-

workers:[83-85] cc-pVTZ, cc-pV(T+d)Z, cc-pVQZ, and cc-pV(Q+d)Z. The larger cc-pV(T+d)Z and cc-pV(Q+d)Z basis sets, which include an extra set of tight *d* functions on second-row atoms (Al-Cl), were only employed for the aluminum atoms. The largest basis set, cc-pV(Q+d)Z, consists of 183 contracted Gaussian functions for the dialuminum monoxide structures. Geometries were optimized at each basis set and level of theory unless stated differently. Harmonic vibrational frequencies were evaluated using analytical methods when available, and otherwise determined through finite differences of gradients or numerical differentiation of total energies.

The electron configurations of the ground state ($X\ ^2\Sigma^+$) and first excited state ($A\ ^2\Pi$) of diatomic AlO may be described as

$$[\text{core}](5\sigma)^2(6\sigma)^2(2\pi)^4(7\sigma) \qquad X\ ^2\Sigma^+ \tag{2.1}$$

and

$$[\text{core}](5\sigma)^2(6\sigma)^2(2\pi)^3(7\sigma)^2 \qquad A\ ^2\Pi \tag{2.2}$$

where [core] designates the six core (Al—1*s*-, 2*s*-, 2*p*-like, O—1*s*-like) orbitals.

As originally noted by Yoshimine, McLean, and Liu[86] in 1973 and recently by Zenouda *et al*.,[87] for the $X\ ^2\Sigma^+$ state of AlO there is no adequate single configuration SCF wave function. This is generally true of open shell system though not for the lowest state of symmetry. Other recent work conducted by Gutsev, Jena, and Bartlett[88] include a coupled cluster study of AlO and its anion. They made no reference to the multireference nature of AlO.

In order to investigate the multireference character of diatomic AlO, symmetric AlOAl, and asymmetric AlAlO molecules, multireference configuration interaction with single and double excitations (MRCISD) wave functions have been constructed. The

complete active space self-consistent field (CASSCF) method has been employed to build the reference wave function for the MRCISD technique. For the diatomic AlO species a full valence active space of [9 electrons/9 molecular orbitals (MOs)] is selected, while for the triatomic molecules a full valence active space of (17 electrons/12 MOs) is chosen. For the $X\ ^2\Sigma^+$ state of AlO the internally contracted MRCISD wave function consists of 200 156 configurations. The dominant configurations of this MRCISD wave function are (with CI coefficients greater than 0.07)

$$\begin{aligned}\Psi_{MRCISD}\left(^2\Sigma^+\right) = 0.935&\left\{[\text{core}](5\sigma)^2(6\sigma)^2(2\pi_x)^2(2\pi_y)^2(7\sigma)\right\}\\ -0.087&\left\{[\text{core}](5\sigma)^2(6\sigma)^2(2\pi_x)^2(2\pi_y)^0(7\sigma)(3\pi_y)^2\right\}\\ -0.087&\left\{[\text{core}](5\sigma)^2(6\sigma)^2(2\pi_x)^0(2\pi_y)^2(7\sigma)(3\pi_x)^2\right\}\\ -0.073&\left\{[\text{core}](5\sigma)^2(6\sigma)^2(2\pi_x)(2\pi_y)(7\sigma)(3\pi_x)(3\pi_y)\right\}\end{aligned} \qquad (2.3)$$

It is clearly seen that the $X\ ^2\Sigma^+$ state of AlO possesses nonnegligible multireference character as pointed out by Yoshimine.[86] Important contributions are from $2\pi\rightarrow3\pi$ double excitations.

Likewise, for the $A\ ^2\Pi$ state of AlO the internally contracted MRCISD wave function consists of 194 933 configurations. The three dominant configurations are

$$\begin{aligned}\Psi_{MRCISD}\left(^2\Pi\right) = 0.943&\left\{[\text{core}](5\sigma)^2(6\sigma)^2(2\pi_x)(2\pi_y)^2(7\sigma)^2\right\}\\ -0.165&\left\{[\text{core}](5\sigma)^2(6\sigma)^2(2\pi_x)(2\pi_y)^2(7\sigma)^0(3\pi_x)^2\right\}\\ -0.072&\left\{[\text{core}](5\sigma)^2(6\sigma)^2(2\pi_x)(2\pi_y)^0(7\sigma)^2(3\pi_y)^2\right\}\end{aligned} \qquad (2.4)$$

The $A\ ^2\Pi$ state of AlO also presents some multireference character. Double excitations of $7\sigma\rightarrow3\pi$ and $2\pi\rightarrow3\pi$ are significant contributions.

The ground state electron configuration of AlOAl ($D_{\infty h}$) may be described as

$$[\text{core}](5\sigma_g)^2(4\sigma_u)^2(2\pi_u)^4(6\sigma_g)^2(5\sigma_u)^2 \qquad \tilde{X}\,{}^1\Sigma_g^+ \tag{2.5}$$

where [core] denotes the 11 core (Al—1*s*-, 2*s*-, 2*p*-like, O—1*s*-like) orbitals. The internally contracted MRCISD wave function includes 5 037 611 configurations. The MRCISD wave function consists of the two major configurations:

$$\begin{aligned}\Psi_{MRCISD}\left({}^1\Sigma_g^+\right) = 0.921&\left\{[\text{core}]\left(5\sigma_g\right)^2\left(4\sigma_u\right)^2\left(2\pi_u\right)^4\left(6\sigma_g\right)^2\left(5\sigma_u\right)^2\right\}\\ -0.084&\left\{[\text{core}]\left(5\sigma_g\right)^2\left(4\sigma_u\right)^2\left(2\pi_u\right)^2\left(6\sigma_g\right)^2\left(5\sigma_u\right)^2\left(3\pi_g\right)^2\right\}\end{aligned} \tag{2.6}$$

The $\tilde{X}\,{}^1\Sigma_g^+$ state of symmetric isomer AlOAl shows some multireference character. The most important excitations in the MRCISD wave function is a $2\pi\rightarrow3\pi$ double excitation. The valence configuration for AlAlO ($C_{\infty v}$) is

$$[\text{core}](8\sigma)^2(9\sigma)^2(3\pi)^4(10\sigma)^2(11\sigma)^2 \qquad \tilde{X}\,{}^1\Sigma^+ \tag{2.7}$$

For the asymmetric AlAlO species the internally contracted MRCISD wave function includes 4 455 513 configurations. The MRCISD wave function has eight configurations with CI coefficients greater than 0.07,

$$\begin{aligned}\Psi_{MRCISD}\left({}^1\Sigma^+\right) = 0.902&\left\{[\text{core}](8\sigma)^2(9\sigma)^2(3\pi)^4(10\sigma)^2(11\sigma)^2\right\}\\ -0.154&\left\{[\text{core}](8\sigma)^2(9\sigma)^2(3\pi)^4(10\sigma)^2(11\sigma)^0\left(4\pi_y\right)^2\right\}\\ -0.154&\left\{[\text{core}](8\sigma)^2(9\sigma)^2(3\pi)^4(10\sigma)^2(11\sigma)^0\left(4\pi_x\right)^2\right\}\\ -0.103&\left\{[\text{core}](8\sigma)^2(9\sigma)^2\left(3\pi_x\right)\left(3\pi_y\right)(10\sigma)^2(11\sigma)^2(4\pi)^0\left(5\pi_x\right)\left(5\pi_y\right)\right\}\\ -0.088&\left\{[\text{core}](8\sigma)^2(9\sigma)^2\left(3\pi_x\right)^0\left(3\pi_y\right)^2(10\sigma)^2(11\sigma)^2(4\pi)^0\left(5\pi_x\right)^2\right\}\\ -0.088&\left\{[\text{core}](8\sigma)^2(9\sigma)^2\left(3\pi_x\right)^2\left(3\pi_y\right)^0(10\sigma)^2(11\sigma)^2(4\pi)^0\left(5\pi_y\right)^2\right\}\\ -0.086&\left\{[\text{core}](8\sigma)^2(9\sigma)^2\left(3\pi_x\right)\left(3\pi_y\right)^2(10\sigma)(11\sigma)^2(4\pi)^0\left(5\pi_x\right)(12\sigma)\right\}\\ -0.086&\left\{[\text{core}](8\sigma)^2(9\sigma)^2\left(3\pi_x\right)^2\left(3\pi_y\right)(10\sigma)(11\sigma)^2(4\pi)^0\left(5\pi_y\right)(12\sigma)\right\}\end{aligned} \tag{2.8}$$

It is evident that the asymmetric isomer AlAlO presents strong multireference character. The major excitations involved in the MRCISD wave functions are $10\sigma\rightarrow4\pi$, $3\pi\rightarrow5\pi$, and $3\pi10\sigma\rightarrow5\pi12\sigma$ double excitations. The transition state for the isomerization reaction AlOAl↔AlAlO on the $^1A'$ surface has the following electron configurations:

$$[\text{core}](10a'')^2(11a')^2(12a')^2(3a'')^2(13a')^2(14a')^2 \qquad {}^1A' \qquad (2.9)$$

The zeroth-order descriptions of the $X\ ^2\Sigma^+$ and $A\ ^2\Pi$ states of AlO, the $\tilde{X}\ ^1\Sigma_g^+$ state of AlOAl and the $\tilde{X}\ ^1\Sigma^+$ state of AlAlO were obtained using single reference SCF (RHF) and CASSCF wave functions. Correlation effects were included using CISD, MRCISD, coupled cluster with single and double excitations (CCSD),[35,89] CCSD with perturbative triples [CCSD(T)],[90,91] CCSD with iterative partial triples [CCSDT-3 (Ref. 46) and CC3 (Ref. 59)], and the full CCSDT levels of theory. In the correlated procedures the six core orbitals were frozen for AlO and 11 core orbitals were frozen for Al_2O. The PSI2,[92] PSI3.2,[93] ACESII,[94] MOLPRO,[95-99] and NWCHEM[100] *ab initio* program packages were utilized during this study.

2.4 RESULTS AND DISCUSSION

In Tables 2.1 and 2.2 total energies and physical properties for the $X\ ^2\Sigma^+$ state and $A\ ^2\Pi$ state of diatomic AlO are presented, respectively. In Figs. 2.1 and 2.2 the optimized geometries for the $\tilde{X}\ ^1\Sigma_g^+$ AlOAl and $\tilde{X}\ ^1\Sigma^+$ AlAlO structures are depicted at eight (seven) levels of sophistication with four basis sets. Total energies and physical properties of these two isomers are presented in Tables 2.3 and 2.4. Figure 2.3 provides the optimized geometries for the $\tilde{X}\ ^1A'$ AlAlO transition state for the isomerization reaction. Total energies and physical properties for this transition state are presented in Table 2.5.

Relative energies for the asymmetric AlAlO with respect to the symmetric AlOAl are shown in Table 2.6. The barrier heights for isomerization between AlOAl and AlAlO through the transition state are available in Table 2.7. Dissociation energies of AlOAl and AlAlO into Al (^{2}P) and $X\ ^2\Sigma^+$ AlO are provided in Table 2.8.

2.4.1 Geometries

The equilibrium bond length for the ground state ($X\ ^2\Sigma^+$) of diatomic AlO is experimentally determined to be r_e(AlO)=1.6179 Å.[61] The theoretically predicted AlO bond length generally increases with advanced treatment of correlation effects and decreases with increase of the basis set size. The inclusion of an extra *d* function on the Al atom shortens the AlO bond distance at all levels of theory. The CCSD method with our largest basis set provides an AlO bond length 0.004 Å less than the experimentally determined r_e value, while the CCSD(T) and CCSDT-3 levels of theory overestimate the AlO bond distance, by 0.011 and 0.013 Å, respectively.

The single electron excitation from the 2π bonding orbital to the nonbonding 7σ orbital shown in Eq. (2.2) clear elongates the AlO bond length for the $A\ ^2\Pi$ state. The predicted AlO bond distances at the correlated levels of theory (Table 2.2) are consistent with the experimentally estimated value of 1.7708 Å (Ref. 61) [CCSD r_e value identical with experiment; CCSD(T) too long by 0.005 Å].

For the symmetric global minimum AlOAl isomer, including electron correlation through coupled cluster and MRCISD methods yields a general trend of increasing AlO bond lengths (Fig. 2.1). The phenomena may be attributed to the 2π (bonding π MO) →3π (nonbonding π MO) double excitation in Eq. (2.6). This bond length is shortened with the increase of the basis set size and the inclusion of an extra *d* function on the Al

atoms. The three coupled cluster methods with single, double, and triple excitations [CCSD(T), CCSDT-3, and CC3] predict similar geometries, as expected. The coupled cluster methods employed in this study predict the AlO bond distance for $\tilde{X}\,^1\Sigma_g^+$ AlOAl is about 0.06 - 0.08 Å longer than that for the $X\ ^2\Sigma^+$ state of AlO, but about 0.06 Å shorter than for the $A\ ^2\Pi$ state of AlO. The recent research of Koput and Gertych[82] for AlOAl predicts an Al-O equilibrium distance of 1.7070 Å [cc-pV5Z CCSD(T) method], compared to the present 1.7077 Å [cc-pV(Q+d)Z CCSD(T) method]. MRCISD geometries agree very well with coupled cluster methods including those of Koput and Gertych.

Also included in Fig. 2.1 are the full CCSDT geometries for AlOAl using the cc-pVTZ and cc-pV(T+d)Z basis sets. The CCSDT distance r_e (Al-O) with the larger basis set is 1.7101 Å very close to the CCSD(T) prediction., 1.7102 Å. The CCSDT-3 (1.7108 Å) and CC3 (1.7124 Å) predictions are a bit further from the full CCSDT Al-O distance.

For the asymmetric AlAlO isomer an improved treatment of correlation effects generally shortens the AlAl bond and elongates the AlO bond as seen in Fig. 2.2. For each respective basis set the inclusion of an extra set of tight *d* functions on the Al atoms again shortens the two bond lengths. The AlO bond distance for AlAlO is significantly shorter than that for the symmetric AlOAl molecule. The three coupled cluster methods [CCSD(T), CCSDT-3, and CC3] provide somewhat larger variations (0.013 Å for Al-Al, 0.027 Å for Al-O) in the geometries for the asymmetric AlAlO isomer than might be expected. The overall molecular size [r_e(AlAl)+r_e(AlO)] for the asymmetric AlAlO is 29% larger than that [two times r_e(AlO)] for the symmetric AlOAl. In this system the AlAl bond is much weaker when compared to the AlO bond. This weak bond lends itself

to be more sensitive to improved treatments of electron correlation which also effects the AlO as shown in Eq. 2.8. The 11σ (nonbonding σ MO) →4π (AlAl bonding π MO) double excitations provide a shorter AlAl bond, while the 3π (AlO bonding π MO) →5π (AlO nonbonding π MO or O 2*p*-like MO) provides a longer AlO bond. The MRCISD method presents the shortest AlAl bond distance among the correlated wave functions.

The transition state structures for the isomerization reaction on the $^1A'$ surface are shown in Fig. 2.3. The AlAl bond distance for the transition state is considerably shorter than the linear AlAlO species, while the AlO bond distance is slightly longer. The transition state has an AlAlO bond angle of around 116°, which is closer to the linear AlAlO equilibrium. The feature is consistent with the Hammond postulate,[101] which states that the transition state has a structure closer to that of the reactant for an exothermic process.

2.4.2 Dipole Moments

Due to molecular symmetry, the symmetric AlOAl isomer does not have a permanent dipole moment. On the other hand, the asymmetric isomer presents a large equilibrium dipole moment, 7.2 D, as seen in Table 2.4. The direction of this dipole moment may be designated as +AlAlO-. The magnitude of predicted dipole moment decreases with advanced treatments of correlation effects, as is often the case. Due to this large dipole moment it may be possible to detect the AlAlO molecule using microwave spectroscopic techniques, when sufficient amounts of AlAlO are produced.

The transition state structure also presents a large dipole moment (6.3 D), as presented in Table 2.5. At this geometry the transition state is nearly as polarized as the

asymmetric AlAlO isomer. This is reasonable since the aluminum atom that is in motion is closer to the other aluminum atom than to the oxygen atom, as suggested by the Hammond postulate.

2.4.3 Harmonic Vibrational Frequencies

The harmonic vibrational frequency for the $X\ ^2\Sigma^+$ ground state of diatomic AlO has been experimentally determined[61] to be 979 cm^{-1}. The vibrational frequencies from the coupled cluster methods are reasonably consistent with the experimental, e.g., ω_e=963 cm^{-1} for the CCSD(T) method with the largest basis set.

Due to the elongated bond length, the vibrational frequency for the $A\ ^2\Pi$ state of AlO is lower than that for the $X\ ^2\Sigma^+$ state. The vibrational frequencies from the correlated wave functions [e.g., 733 cm^{-1} for the cc-pV(Q+d)Z CCSD(T) method] are in good agreement with the experimental value of 728.5 cm^{-1}.[61]

The three harmonic vibrational frequencies for the $\tilde{X}\ ^1\Sigma_g^+$ AlOAl molecule are predicated to be lower with the correlated wave functions relative to those with the SCF method, reflecting the longer AlO bond length with correlated methods. The three coupled cluster techniques with single, double, and triple excitations [CCSD(T), CCSDT-3, and CC3] present very similar vibrational frequencies. The predicted frequencies for the symmetric AlOAl isomer at the cc-pV(Q+d)Z CCSD(T) level of theory (in Table 2.3) are ω_1=517 cm^{-1}, ω_2=95 cm^{-1}, and ω_3=1014 cm^{-1}, which compare well to the experimental fundamental frequencies in the gas phase[72] of ν_1=515 cm^{-1}, ν_2=99 cm^{-1}, and ν_3=992 cm^{-1}, respectively. For comparison, Koput and Gertych[82] predict 519, 97, and 1016 cm^{-1}, respectively, for the three AlOAl frequencies.

The predicted harmonic vibrational frequencies for the asymmetric AlAlO isomer at the cc-pV(Q+d)Z CCSD(T) level of theory (in Table 2.4) are ω_1=1042 cm^{-1}, ω_2=73 cm^{-1}, and ω_3=253 cm^{-1}. No experiments have been reported for AlAlO ($C_{\infty v}$) with which to compare. The AlO stretching ω_1 mode for AlAlO presents a higher frequency than that for the $A\ ^2\Pi$ state of diatomic AlO. This feature is consistent with Badger's rule,[102,103] that the larger force constant (higher vibrational frequency) may be associated with the shorter bond length. As mentioned above the weak AlAl bond is quite sensitive to advanced treatments of electron correlation. The inclusion of the higher order triples excitations results in a strong AlAl bond and a resultant weaker AlO bond as seen in the reduction of the ω_1 mode from 1098 cm^{-1} at the cc-pV(Q+d)Z CCSD to 875 cm^{-1} at the cc-pV(Q+d)Z CC3 levels of theory.

Harmonic vibrational frequencies for the transition state are provided in Table 2.5. The predicted frequencies at the cc-pV(Q+d)Z CCSD(T) level of theory are ω_1=1011 cm^{-1}, ω_2=291 cm^{-1}, and ω_3=102*i* cm^{-1}. The AlAl stretching ω_3 frequency for the transition state is higher than that for the linear AlAlO molecule, reflecting the shorter AlAl bond distance.

2.4.4 Infrared (IR) Intensities

IR intensities were determined using analytical derivative methods for SCF and with frozen core orbital for the CCSD and CCSD(T) levels of theory. Tables 2.3 and 2.4 contain IR intensities for the SCF, CCSD, and CCSD(T) levels of theory for both AlOAl and AlAlO, respectively. The $\omega_1(\sigma_g^+)$ symmetric stretching frequency of AlOAl is IR inactive and hence would be difficult to detect with conventional IR spectroscopy.

For symmetric AlOAl, the SCF method predicts an extremely weak IR intensity of ~0.01 km mol^{-1} for the $\omega_2(\pi_u)$ bending mode. With the inclusion of electron correlation via the CCSD and CCSD(T) methods, the IR intensity of $\omega_2(\pi_u)$ increases to a value of ~0.5 km mol^{-1} at both the cc-pV(T+d)Z CCSD and cc-pV(T+d)Z CCSD(T) levels of theory. For $\omega_3(\sigma_u^+)$ asymmetric stretching mode the IR intensity is predicted to be 700 km mol^{-1} at the SCF level with the cc-pV(Q+d)Z basis, and 625 km mol^{-1} at the CCSD level and 602 km mol^{-1} at the CCSD(T) level with the cc-pV(T+d)Z basis. With the increase of electron correlation effects the ω_3 IR intensity is reduced. Since the ω_2 mode presents a low frequency of about 100 cm^{-1} and its IR intensity is about three orders of magnitude smaller than that of the asymmetric stretching ω_3 mode, it is well understandable that earlier spectroscopists had difficulty in detecting the ν_2 mode of AlOAl.

For asymmetric AlAlO, with the inclusion of electron correlation effects, the IR intensities of all three vibrational modes are reduced significantly. At the CCSD(T) cc-pV(T+d)Z level (in Table 2.4) the predicted IR intensities are for the AlO stretching frequency $\omega_1(\sigma^+)$, 1.8 km mol^{-1}; the AlAl stretching frequency $\omega_3(\sigma^+)$, 52 km mol^{-1}; and the bending frequency $\omega_2(\pi)$, 52 km mol^{-1}. Due to the substantial IR intensities, the vibrational fundamentals ν_1 and ν_3 for AlAlO should be detectable using IR spectroscopic techniques.

2.4.5 Energetics

For the diatomic AlO molecule the $A\ ^2\Pi$-$X\ ^2\Sigma^+$ energy splitting (T_e value) is experimentally known to be 5341.7 cm^{-1} ($^2\Pi_{3/2}$; 15.27 kcal mol^{-1}, 0.6623 eV).[61] Our

theoretical predictions of T_e=14.3 kcal mol^{-1} at the cc-pV(Q+d)Z CCSD(T), 15.6 kcal mol^{-1} at the cc-pV(Q+d)Z CCSDT-3, and 15.6 kcal mol^{-1} at the cc-pV(Q+d)Z MRCISD level of theory (in Table 2.2) agree very well with the experimental values.

Relative energies between the ground state of the two dialuminum monoxide isomers are given in Table 2.4. With the cc-pV(Q+d)Z basis set the classical relative energies T_e for the asymmetric isomer AlAlO with respect to the symmetric isomer AlOAl are predicted to be 95.4 (SCF), 88.7 (CISD), 86.5 (MRCISD), 86.2 (CCSD), 82.3 [CCSD(T)], 80.6 (CCSDT-3), and 78.6 kcal mol^{-1} (CC3). The energy separation generally decreases with the level of sophistication. The inclusion of zero point vibrational energy (ZPVE) slightly lowers the relative energy between these isomers. Our predicted energy difference of 82 kcal mol^{-1} at the cc-pV(Q+d)Z CCSD(T) level of theory is 12 kcal mol^{-1} smaller than the earlier value of 94 kcal mol^{-1} at the unrestricted Hartree-Fock (UHF)/6-31G* level of theory.[80]

The ZPVE corrected barrier height for the isomerization reaction AlOAl→AlAlO is predicted to be 84.3 [cc-pV(Q+d)Z CCSD(T)] while the activation energy for the reverse reaction AlAlO→AlOAl is evaluated to be only 2.4 kcal mol^{-1} [cc-pV(Q+d)Z CCSD(T)]. Therefore, the forward isomerization reaction is unlikely to occur at room temperature, while the reverse isomerization reaction may be expected at low temperatures. Schematic potential energy surface at the cc-pV(Q+d)Z CCSD(T) level of theory is depicted in Fig 2.4.

2.4.6 Dissociation Energies

Dissociation energies from the ground state of the two isomers to atomic aluminum (^{2}P) plus diatomic aluminum monoxide ($X\ ^2\Sigma^+$) are reported in Table 1.8. It was found that the SCF method does not predicted $^2\Sigma^+$ AlO to be the electronic ground state of the diatomic. When electron correlation is includes [MRCISD, CCSD, CCSD(T), CCSDT-3, and CC3] the theory correctly predicts the $^2\Sigma^+$ state to be the lowest in energy for AlO. The two dissociation reactions studied are

$$\mathrm{AlOAl}(\tilde{X}\ ^1\Sigma_g^+) \rightarrow \mathrm{Al}(^2\mathrm{P}) + \mathrm{AlO}(X\ ^2\Sigma^+)$$

$$\mathrm{AlAlO}(\tilde{X}\ ^1\Sigma^+) \rightarrow \mathrm{Al}(^2\mathrm{P}) + \mathrm{AlO}(X\ ^2\Sigma^+)$$

At the cc-pV(Q+d)Z CCSD(T) level of theory the dissociation energy with the ZPVE correction is predicted to be 130.8 kcal mol^{-1} for the first and 48.9 kcal mol^{-1} for the second reaction. The dissociation energy of 130.8 kcal mol^{-1} for the symmetric isomer (AlOAl→AlAlO) is in good agreement with the experimental value of 128.8 ± 1.3 kcal mol^{-1}.[104,105] From our systematic study it can be estimated that these predicted dissociation energies have an uncertainty of 2 kcal mol^{-1}. Since the dissociation energy for the asymmetric isomer is only 38% of the symmetric isomer, the sensitive nature of predicting the weak Al-Al bond distance is to be expected.

2.5 CONCLUDING REMARKS

The singlet electronic ground state isomers ($\tilde{X}\ ^1\Sigma_g^+$ AlOAl and $\tilde{X}\ ^1\Sigma^+$ AlAlO) of dialuminum monoxide have been studied using *ab initio* electronic structure theory. The two isomers are confirmed to have linear structures at all levels of theory. At the cc-pV(Q+d)Z CCSD(T) level of theory the $\tilde{X}\ ^1\Sigma_g^+$ state of AlOAl is predicted to have the

following harmonic vibrational frequencies ω_1=517 cm^{-1}, ω_2=95 cm^{-1}, and ω_3=1041 cm^{-1}, which compare well to the experimental gas phase fundamental frequencies of ν_1=525 cm^{-1}, ν_2=99 cm^{-1}, and ν_3=992 cm^{-1}, respectively. At the cc-pV(Q+d)Z CCSD(T) level of theory the $\tilde{X}\,^1\Sigma^+$ state of AlAlO presents the harmonic vibrational frequencies of ω_1=1042 cm^{-1}, ω_2=73 cm^{-1}, ω_3=253 cm^{-1}. No experimental values have been reported to date for these AlAlO vibrational frequencies. The symmetric isomer AlOAl is predicted to lie 81.9 kcal mol^{-1} below the asymmetric isomer AlAlO at the cc-pV(Q+d)Z CCSD(T) level of theory. Our dissociation energy of 130.8 kcal mol^{-1} predicted for $\mathrm{AlOAl}(\tilde{X}\,^1\Sigma_g^+) \rightarrow \mathrm{Al}(^2\mathrm{P}) + \mathrm{AlO}(X\,^2\Sigma^+)$ is in good agreement with the experimental finding of 128.8 ± 1.3 kcal mol^{-1}. The value of 48.9 kcal mol^{-1} for the reaction $\mathrm{AlAlO}(\tilde{X}\,^1\Sigma^+) \rightarrow \mathrm{Al}(^2\mathrm{P}) + \mathrm{AlO}(X\,^2\Sigma^+)$ of the asymmetric isomer would suggest that this isomer might be synthesized and captured in cryogenic matrices for spectroscopic studies.

2.6 ACKNOWLEDGEMENTS

This research was supported by the U.S. National Science Foundation, Grant No. CHE-0136186. The authors would like to thank Steven E. Wheeler for his assistance with the schematic potential energy surface and Nathan J. DeYonker for his expertise with MRCISD. A portion of the research described in this paper was performed in the Environmental Molecular Studies Laboratory, a national scientific user facility sponsored by the Department of Energy's Office of Biological and Environmental Research and located at Pacific Northwest National Laboratory.

Table 2.1: Total energies (in hartree), dipole moments (in debye), harmonic vibrational frequencies (in cm^{-1}), infrared (IR) intensities (in km mol^{-1}), and ZPVE (in kcal mol^{-1}) for the ground state ($X\ ^2\Sigma^+$) of AlO.

Level of Theory	Total Energy	r(AlO)	μ_e	ω_e	ZPVE
cc-pVTZ SCF	-316.769 301	1.7010	1.94	783 (103)	1.12
cc-pV(T+d)Z SCF	-316.771 223	1.6902	1.89	789 (97)	1.13
cc-pVQZ SCF	-316.778 957	1.6928	1.98	793 (103)	1.13
cc-pV(Q+d)Z SCF	-316.779 820	1.6890	1.96	794 (100)	1.14
cc-pVTZ CCSD	-317.065 688	1.6281	-	942	1.35
cc-pV(T+d)Z CCSD	-317.069 698	1.6179	-	970	1.39
cc-pVQZ CCSD	-317.095 307	1.6191	-	979	1.40
cc-pV(Q+d)Z CCSD	-317.096 796	1.6141	-	976	1.40
cc-pVTZ CCSD(T)	-317.085 528	1.6405	-	965	1.38
cc-pV(T+d)Z CCSD(T)	-317.088 261	1.6371	-	992	1.42
cc-pVQZ CCSD(T)	-317.116 641	1.6331	-	971	1.39
cc-pV(Q+d)Z CCSD(T)	-317.117 938	1.6289	-	963	1.38
cc-pVTZ CCSDT-3	-317.087 777	1.6414	-	992	1.42
cc-pV(T+d)Z CCSDT-3	-317.089 417	1.6391	-	915	1.31
cc-pVQZ CCSDT-3	-317.118 690	1.6345	-	988	1.41
cc-pV(Q+d)Z CCSDT-3	-317.119 965	1.6307	-	952	1.36
cc-pVTZ CC3	-317.092 154	1.6452	-	1032	1.48
cc-pV(T+d)Z CC3	-317.094 737	1.6377	-	994	1.42
cc-pVQZ CC3	-317.123 091	1.6392	-	1003	1.43
cc-pV(Q+d)Z CC3	-317.124 306	1.6358	-	991	1.42
cc-pVTZ CCSDT	-317.085 308	1.6377			
cc-pV(T+d)Z CCSDT	-317.088 165	1.6279			
cc-pVTZ MRCISD	-317.074 383	1.6360			
cc-pV(T+d)Z MRCISD	-317.077 265	1.6261			
cc-pVQZ MRCISD	-317.103 556	1.6286			
cc-pV(Q+d)Z MRCISD	-317.104 949	1.6240			
Experiment, Ref. 61		1.6179		979	

Table 2.2: Total energies (in hartree), dipole moments (in debye), harmonic vibrational frequencies (in cm^{-1}), infrared (IR) intensities (in km mol^{-1}), ZPVE (in kcal mol^{-1}), and the T_e values (in kcal mol^{-1}) for the first excited state ($A\ ^2\Pi$) of AlO.

Level of Theory	Total Energy	r(AlO)	μ_e	ω_e	ZPVE	T_e
cc-pVTZ SCF	-316.791 589	1.7607	1.28	768 (120)	1.10	-13.99
cc-pV(T+d)Z SCF	-316.793 340	1.7513	1.25	773 (117)	1.10	-13.88
cc-pVQZ SCF	-316.800 914	1.7537	1.31	776 (123)	1.11	-13.78
cc-pV(Q+d)Z SCF	-316.801 731	1.7504	1.30	777 (123)	1.11	-13.75
cc-pVTZ CCSD	-317.057 208	1.7812	-	737	1.05	5.32
cc-pV(T+d)Z CCSD	-317.058 907	1.7718	-	741	1.06	6.77
cc-pVQZ CCSD	-317.084 581	1.7742	-	742	1.06	6.73
cc-pV(Q+d)Z CCSD	-317.085 418	1.7709	-	744	1.06	7.14
cc-pVTZ CCSD(T)	-317.065 626	1.7858	-	727	1.04	12.49
cc-pV(T+d)Z CCSD(T)	-317.067 289	1.7764	-	731	1.05	13.16
cc-pVQZ CCSD(T)	-317.094 327	1.7795	-	731	1.05	14.00
cc-pV(Q+d)Z CCSD(T)	-317.095 150	1.7762	-	733	1.05	14.30
cc-pVTZ CCSDT-3	-317.065 541	1.7868	-	724	1.04	13.95
cc-pV(T+d)Z CCSDT-3	-317.067 195	1.7773	-	728	1.04	13.94
cc-pVQZ CCSDT-3	-317.094 240	1.7804	-	729	1.04	15.34
cc-pV(Q+d)Z CCSDT-3	-317.095 061	1.7771	-	730	1.04	15.63
cc-pVTZ CC3	-317.066 278	1.7876	-	722	1.03	16.24
cc-pV(T+d)Z CC3	-317.067 252	1.7781	-	726	1.04	17.25
cc-pVQZ CC3	-317.095 056	1.7813	-	727	1.04	17.59
cc-pV(Q+d)Z CC3	-317.095 874	1.7780	-	728	1.04	17.84
cc-pV(T+d)Z CCSDT	-317.067 959	1.7769				12.68
cc-pVTZ MRCISD	-317.052 588	1.7859				13.68
cc-pV(T+d)Z MRCISD	-317.054 210	1.7768				14.47
cc-pVQZ MRCISD	-317.079 221	1.7792				15.27
cc-pV(Q+d)Z MRCISD	-317.080 023	1.7759				15.64
Experiment, Ref. 61		1.7708		729		15.27

Table 2.3: Total energies (in hartree), harmonic vibrational frequencies (in cm^{-1}), infrared (IR) intensities (in km mol^{-1}), and zero-point vibrational energies (ZPVE) (in kcal mol^{-1}) for the linear equilibrium geometry ($\tilde{X}\ ^1\Sigma_g^+$ state) of AlOAl. IR intensities of the ω_2 mode were doubled.

Level of Theory	Total Energy	$\omega_1(\sigma_g^+)$	$\omega_2(\pi_u)$	$\omega_3(\sigma_u^+)$	ZPVE
cc-pVTZ SCF	-558.847 020	545 (0)	126 (0.0_3)	1063 (700)	2.66
cc-pV(T+d)Z SCF	-558.851 241	548 (0)	127 (0.0_{03})	1067 (695)	2.67
cc-pVQZ SCF	-558.860 315	552 (0)	126 (0.0_1)	1073 (699)	2.68
cc-pV(Q+d)Z SCF	-558.862 372	552 (0)	127 (0.0_{05})	1074 (700)	2.69
cc-pVTZ CISD	-559.170 048	529 (0)	110 (0.4)	1033 (648)	2.55
cc-pV(T+d)Z CISD	-559.174 106	531 (0)	110 (0.3)	1036 (642)	2.55
cc-pVQZ CISD	-559.202 946	534	105	1042	2.55
cc-pV(Q+d)Z CISD	-559.205 004	535	106	1043	2.56
cc-pVTZ CCSD	-559.208 490	522 (0)	105 (0.2)	1019 (630)	2.50
cc-pV(T+d)Z CCSD	-559.212 513	522 (0)	105 (0.5)	1015 (625)	2.50
cc-pVQZ CCSD	-559.243 161	525	108	1026	2.53
cc-pV(Q+d)Z CCSD	-559.245 206	526	104	1029	2.52
cc-pVTZ CCSD(T)	-559.223 392	512 (0)	98 (0.7)	1005 (607)	2.45
cc-pV(T+d)Z CCSD(T)	-559.227 307	513 (0)	95 (0.5)	1001 (602)	2.43
cc-pVQZ CCSD(T)	-559.259 913	516	95	1014	2.46
cc-pV(Q+d)Z CCSD(T)	-559.261 912	517	95	1014	2.46
cc-pVTZ CCSDT-3	-559.223 028	509	95	1002	2.43
cc-pV(T+d)Z CCSDT-3	-559.226 926	511	95	1005	2.44
cc-pVQZ CCSDT-3	-559.259 515	515	96	1012	2.46
cc-pV(Q+d)Z CCSDT-3	-559.261 510	515	94	1012	2.45
cc-pVTZ CC3	-559.224 927	506	94	998	2.42
cc-pV(T+d)Z CC3	-559.228 789	508	94	1001	2.43
cc-pVQZ CC3	-559.261 533	511	93	1007	2.44
cc-pV(Q+d)Z CC3	-559.263 512	512	93	1008	2.44
cc-pVTZ CCSDT	-559.223 588				
cc-pV(T+d)Z CCSDT	-559.227 502				
cc-pVTZ MRCISD	-559.204 310				
cc-pV(T+d)Z MRCISD	-559.208 151				
cc-pVQZ MRCISD	-559.237 932				
cc-pV(Q+d)Z MRCISD	-559.239 892				
Experiment Ref. 71	(gas phase)	525	99	992	
Ref. 69	(matrix)	471			
Ref. 64,66,68,70	(matrix)			992.8	
Ref. 64,66	(matrix)			989.4	
Ref. 61,70	(matrix)			991	

Table 2.4: Total energies (in hartree), dipole moments (in debye), harmonic vibrational frequencies (in cm^{-1}), infrared (IR) intensities (in km mol^{-1}), and zero-point vibrational energies (ZPVE) (in kcal mol^{-1}) for the linear geometry ($\tilde{X}\,^1\Sigma^+$ state) of AlAlO. IR intensities of the ω_2 mode were doubled.

Level of Theory	Total Energy	μ_e	$\omega_1(\sigma^+)$	$\omega_2(\pi)$	$\omega_3(\sigma^+)$	ZPVE
cc-pVTZ SCF	-558.695 921	8.44	1191 (84)	106 (99)	251 (68)	2.36
cc-pV(T+d)Z SCF	-558.700 195	8.38	1200 (86)	105 (100)	251 (67)	2.37
cc-pVQZ SCF	-558.708 319	8.68	1194 (99)	105 (105)	249 (69)	2.36
cc-pV(Q+d)Z SCF	-558.710 364	8.63	1195 (101)	105 (106)	249 (68)	2.36
cc-pVTZ CISD	-559.030 143	7.98	1126 (34)	96 (75)	260 (60)	2.26
cc-pV(T+d)Z CISD	-559.033 868	7.96	1134 (34)	95 (76)	260 (59)	2.26
cc-pVQZ CISD	-559.061 809	-	1130	94	258	2.25
cc-pV(Q+d)Z CISD	-559.063 642	-	1131	94	258	2.26
cc-pVTZ CCSD	-559.072 742	7.68	1092 (21)	85 (64)	259 (55)	2.17
cc-pV(T+d)Z CCSD	-559.076 290	7.65	1100 (21)	84 (65)	259 (54)	2.18
cc-pVQZ CCSD	-559.106 133	-	1098	83	255	2.17
cc-pV(Q+d)Z CCSD	-559.107 880	-	1098	83	255	2.17
cc-pVTZ CCSD(T)	-559.094 208	7.17	1030 (1.6)	75 (50)	256 (53)	2.05
cc-pV(T+d)Z CCSD(T)	-559.097 344	7.19	1041 (1.8)	75 (52)	257 (52)	2.07
cc-pVQZ CCSD(T)	-559.129 184	-	1040	73	253	2.06
cc-pV(Q+d)Z CCSD(T)	-559.130 734	-	1042	73	253	2.06
cc-pVTZ CCSDT-3	-559.097 128	-	964	70	256	1.94
cc-pV(T+d)Z CCSDT-3	-559.099 976	-	977	70	256	1.96
cc-pVQZ CCSDT-3	-559.131 614	-	986	69	252	1.97
cc-pV(Q+d)Z CCSDT-3	-559.133 042	-	989	68	252	1.97
cc-pVTZ CC3	-559.103 132	-	784	66	255	1.67
cc-pV(T+d)Z CC3	-559.105 492	-	830	67	255	1.74
cc-pVQZ CC3	-559.137 110	-	863	58	251	1.76
cc-pV(Q+d)Z CC3	-559.138 340	-	875	58	251	1.78
cc-pVTZ MRCISD	-559.070 042					
cc-pV(T+d)Z MRCISD	-559.072 014					
cc-pVQZ MRCISD	-559.101 124					
cc-pV(Q+d)Z MRCISD	-559.102 001					

Table 2.5: Total energies (in hartree), bond distances (in Å), and angles (in degrees), dipole moments (in debye), harmonic vibrational frequencies (in cm^{-1}), infrared (IR) intensities (in km mol^{-1}), and zero-point vibrational energies (ZPVE) (in kcal mol^{-1}) for the isomerization transition state ($\tilde{X}\,^1A'$ state) of AlAlO.

Level of Theory	Total Energy	r(AlO)	r(AlAl)	θ(AlAlO)	μ_e	ω_1(a′)	ω_2(a′)	ω_3(a′)	ZPVE
cc-pVTZ SCF	-558.684 379	1.5874	2.7563	105.56	7.10	1160 (87.9)	282 (63)	151*i*	2.06
cc-pV(T+d)Z SCF	-558.688 940	1.5787	2.7528	105.57	7.04	1171 (88.7)	283 (63)	150*i*	2.08
cc-pVQZ SCF	-558.697 146	1.5829	2.7550	105.66	-	1171	268	150*i*	2.06
cc-pV(Q+d)Z SCF	-558.699 294	1.5800	2.7557	105.37	-	1168	267	150*i*	2.05
cc-pVTZ CCSD	-559.065 797	1.6200	2.7194	111.00	6.60	1060 (23.9)	295 (39)	122*i*	1.94
cc-pV(T+d)Z CCSD	-559.069 591	1.6111	2.7174	111.27	6.59	1070 (23.7)	296 (38)	122*i*	1.95
cc-pVQZ CCSD	-559.099 685	1.6174	2.7185	111.44	-	1063	294	115*i*	1.94
cc-pV(Q+d)Z CCSD	-559.101 549	1.6108	2.7172	111.57	-	1072	294	119*i*	1.95
cc-pVTZ CCSD(T)	-559.089 400	1.6372	2.7190	115.39	6.24	994 (1.59)	293 (36)	106*i*	1.84
cc-pV(T+d)Z CCSD(T)	-559.092 726	1.6278	2.7179	115.77	6.29	1005 (1.57)	293 (36)	105*i*	1.86
cc-pVQZ CCSD(T)	-559.124 485	1.6310	2.7201	116.45	-	1009	291	102*i*	1.86
cc-pV(Q+d)Z CCSD(T)	-559.126 571	1.6270	2.7193	116.65	-	1011	291	102*i*	1.86
cc-pVTZ CCSDT-3[a]	-559.092 643								
cc-pV(T+d)Z CCSDT-3[a]	-559.095 669								
cc-pVQZ CCSDT-3[a]	-559.127 727								
cc-pV(Q+d)Z CCSDT-3[a]	-559.129 235								
cc-pVTZ CC3[a]	-559.098 928								
cc-pV(T+d)Z CC3[a]	-559.101 517								
cc-pVQZ CC3[a]	-559.133 699								
cc-pV(Q+d)Z CC3[a]	-559.135 015								

[a] CCSDT-3 and CC3 total energies were obtained using the CCSD(T) geometry of the corresponding basis set.

Table 2.6: Relative energies of the asymmetric AlAlO structure with respect to the symmetric AlOAl structure in kcal mol^{-1}, with zero point vibrational energy corrected values in parentheses.

Level of Theory	Relative Energy	
cc-pVTZ SCF	94.82	(94.52)
cc-pV(T+d)Z SCF	94.78	(94.49)
cc-pVQZ SCF	95.38	(95.06)
cc-pV(Q+d)Z SCF	95.39	(95.06)
cc-pVTZ CISD	87.79	(87.50)
cc-pV(T+d)Z CISD	88.00	(87.71)
cc-pVQZ CISD	88.56	(88.26)
cc-pV(Q+d)Z CISD	88.71	(88.41)
cc-pVTZ CCSD	85.18	(84.85)
cc-pV(T+d)Z CCSD	85.48	(85.17)
cc-pVQZ CCSD	85.99	(85.63)
cc-pV(Q+d)Z CCSD	86.17	(85.82)
cc-pVTZ CCSD(T)	81.06	(80.67)
cc-pV(T+d)Z CCSD(T)	81.55	(81.19)
cc-pVQZ CCSD(T)	82.03	(81.63)
cc-pV(Q+d)Z CCSD(T)	82.32	(81.92)
cc-pVTZ CCSDT-3	79.00	(78.52)
cc-pV(T+d)Z CCSDT-3	79.66	(79.19)
cc-pVQZ CCSDT-3	80.26	(79.77)
cc-pV(Q+d)Z CCSDT-3	80.61	(80.13)
cc-pVTZ CC3	76.43	(75.68)
cc-pV(T+d)Z CC3	77.37	(76.69)
cc-pVQZ CC3	78.08	(77.40)
cc-pV(Q+d)Z CC3	78.55	(77.88)
cc-pVTZ MRCISD	84.25	
cc-pV(T+d)Z MRCISD	85.43	
cc-pVQZ MRCISD	85.85	
cc-pV(Q+d)Z MRCISD	86.52	

Table 2.7: Barrier heights for the isomerization (in kcal mol^{-1}) between AlOAl and AlAlO. Zero-point vibrational energy corrected values in parentheses.

Level of Theory	AlOAl→AlAlO	AlAlO→AlOAl
cc-pVTZ SCF	102.06 (101.46)	7.24 (6.94)
cc-pV(T+d)Z SCF	101.85 (101.25)	7.06 (6.77)
cc-pVQZ SCF	102.39 (101.76)	7.01 (6.71)
cc-pV(Q+d)Z SCF	102.33 (101.70)	6.95 (6.63)
cc-pVTZ CCSD	89.54 (88.98)	4.36 (4.12)
cc-pV(T+d)Z CCSD	89.69 (89.14)	4.20 (3.97)
cc-pVQZ CCSD	90.03 (89.45)	4.05 (3.81)
cc-pV(Q+d)Z CCSD	90.15 (89.58)	3.97 (3.75)
cc-pVTZ CCSD(T)	84.08 (83.47)	3.02 (2.80)
cc-pV(T+d)Z CCSD(T)	84.45 (83.87)	2.90 (2.68)
cc-pVQZ CCSD(T)	84.98 (84.38)	2.95 (2.75)
cc-pV(Q+d)Z CCSD(T)	84.93 (84.33)	2.61 (2.41)
cc-pVTZ CCSDT-3[a]	81.82 (81.23)	2.81 (2.71)
cc-pV(T+d)Z CCSDT-3[a]	82.37 (81.78)	2.70 (2.60)
cc-pVQZ CCSDT-3[a]	82.70 (82.10)	2.44 (2.33)
cc-pV(Q+d)Z CCSDT-3[a]	83.00 (82.41)	2.39 (2.28)
cc-pVTZ CC3[a]	79.07 (78.49)	2.64 (2.80)
cc-pV(T+d)Z CC3[a]	79.86 (79.29)	2.49 (2.61)
cc-pVQZ CC3[a]	80.22 (79.64)	2.14 (2.24)
cc-pV(Q+d)Z CC3[a]	80.63 (80.05)	2.09 (2.17)

[a] The ZPVE from the CCSD(T) method with the corresponding basis set was used to obtain zero-point corrected values for CCSDT-3 and CC3.

Table 2.8: Dissociation energies of symmetric AlOAl and asymmetric AlAlO into atomic Al (^{2}P) plus AlO (X $^2\Sigma^+$) in kcal mol^{-1}. Zero-point vibrational energy corrected values in parentheses.

Level of Theory	Al (^{2}P)	AlO ($X\,^2\Sigma^+$)	D_e (D_0) AlOAl	D_e (D_0) AlAlO
cc-pVTZ SCF	-241.875 131	-316.769 301	127.13 (125.59)	32.31 (31.06)
cc-pV(T+d)Z SCF	-241.875 141	-316.771 223	128.56 (127.02)	33.78 (32.53)
cc-pVQZ SCF	-241.876 477	-316.778 957	128.56 (127.01)	33.19 (31.96)
cc-pV(Q+d)Z SCF	-241.876 484	-316.779 820	129.31 (127.76)	33.92 (32.69)
cc-pVTZ CCSD	-241.929 846	-317.065 688	133.63 (132.48)	48.45 (47.62)
cc-pV(T+d)Z CCSD	-241.929 945	-317.069 698	133.58 (132.47)	48.10 (47.30)
cc-pVQZ CCSD	-241.932 191	-317.095 307	135.33 (134.20)	49.34 (48.57)
cc-pV(Q+d)Z CCSD	-241.932 257	-317.096 796	135.64 (134.51)	49.46 (48.69)
cc-pVTZ CCSD(T)	-241.931 175	-317.085 528	129.70 (128.63)	48.64 (47.96)
cc-pV(T+d)Z CCSD(T)	-241.931 283	-317.088 261	130.37 (129.36)	48.82 (48.17)
cc-pVQZ CCSD(T)	-241.933 664	-317.116 641	131.53 (130.46)	49.50 (48.83)
cc-pV(Q+d)Z CCSD(T)	-241.933 735	-317.117 938	131.93 (130.84)	49.61 (48.93)
cc-pVTZ CCSDT-3	-241.931 155	-317.087 777	128.07 (127.06)	49.07 (48.54)
cc-pV(T+d)Z CCSDT-3	-241.931 263	-317.089 417	129.42 (128.29)	49.76 (49.10)
cc-pVQZ CCSDT-3	-241.933 648	-317.118 690	130.01 (128.96)	49.75 (49.19)
cc-pV(Q+d)Z CCSDT-3	-241.933 720	-317.119 965	130.41 (129.32)	49.80 (49.19)
cc-pVTZ CC3	-241.931 126	-317.092 154	126.54 (125.59)	50.11 (49.91)
cc-pV(T+d)Z CC3	-241.931 233	-317.094 737	127.27 (126.27)	49.90 (49.58)
cc-pVQZ CC3	-241.933 618	-317.123 091	128.53 (127.53)	50.45 (50.13)
cc-pV(Q+d)Z CC3	-241.933 690	-317.124 306	128.96 (127.94)	50.42 (50.06)
Experiment[104,105]			128.8 ± 1.3	

1.6931	cc-pVTZ SCF
1.6845	cc-pV(T+d)Z SCF
1.6857	cc-pVQZ SCF
1.6823	cc-pV(Q+d)Z SCF
1.7071	cc-pVTZ CISD
1.6986	cc-pV(T+d)Z CISD
1.6989	cc-pVQZ CISD
1.6955	cc-pV(Q+d)Z CISD
1.7134	cc-pVTZ CCSD
1.7048	cc-pV(T+d)Z CCSD
1.7052	cc-pVQZ CCSD
1.7018	cc-pV(Q+d)Z CCSD
1.7189	cc-pVTZ CCSD(T)
1.7102	cc-pV(T+d)Z CCSD(T)
1.7111	cc-pVQZ CCSD(T)
1.7077	cc-pV(Q+d)Z CCSD(T)
1.7195	cc-pVTZ CCSDT-3
1.7108	cc-pV(T+d)Z CCSDT-3
1.7116	cc-pVQZ CCSDT-3
1.7082	cc-pV(Q+d)Z CCSDT-3
1.7211	cc-pVTZ CC3
1.7124	cc-pV(T+d)Z CC3
1.7133	cc-pVQZ CC3
1.7099	cc-pV(Q+d)Z CC3
1.7187	cc-pVTZ CCSDT
1.7101	cc-pV(T+d)Z CCSDT
1.7190	cc-pVTZ MRCISD
1.7101	cc-pV(T+d)Z MRCISD
1.7107	cc-pVQZ MRCISD
1.7072	cc-pV(Q+d)Z MRCISD

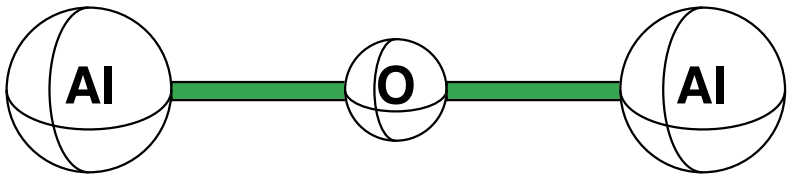

Figure 2.1: Predicted geometries for the $\tilde{X}\,^1\Sigma_g^+$ state of AlOAl at eight levels of sophistication with the four basis sets. Bond lengths are in Å.

cc-pVTZ SCF	2.8387	1.5799
cc-pV(T+d)Z SCF	2.8378	1.5716
cc-pVQZ SCF	2.8442	1.5768
cc-pV(Q+d)Z SCF	2.8434	1.5728
cc-pVTZ CISD	2.7994	1.6019
cc-pV(T+d)Z CISD	2.7984	1.5937
cc-pVQZ CISD	2.8041	1.5975
cc-pV(Q+d)Z CISD	2.8032	1.5937
cc-pVTZ CCSD	2.7919	1.6124
cc-pV(T+d)Z CCSD	2.7910	1.6041
cc-pVQZ CCSD	2.7976	1.6077
cc-pV(Q+d)Z CCSD	2.7967	1.6040
cc-pVTZ CCSD(T)	2.7866	1.6281
cc-pV(T+d)Z CCSD(T)	2.7861	1.6195
cc-pVQZ CCSD(T)	2.7933	1.6230
cc-pV(Q+d)Z CCSD(T)	2.7927	1.6191
cc-pVTZ CCSDT-3	2.7808	1.6402
cc-pV(T+d)Z CCSDT-3	2.7810	1.6305
cc-pVQZ CCSDT-3	2.7881	1.6328
cc-pV(Q+d)Z CCSDT-3	2.7878	1.6286
cc-pVTZ CC3	2.7691	1.6656
cc-pV(T+d)Z CC3	2.7716	1.6518
cc-pVQZ CC3	2.7792	1.6414
cc-pV(Q+d)Z CC3	2.7798	1.6461
cc-pVTZ MRCISD	2.7007	1.6534
cc-pV(T+d)Z MRCISD	2.6896	1.6511
cc-pVQZ MRCISD	2.6848	1.6548
cc-pV(Q+d)Z MRCISD	2.6747	1.6544

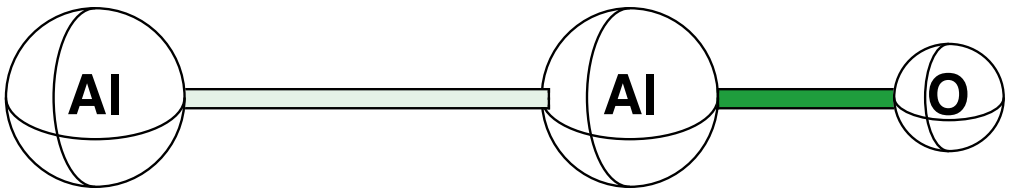

Figure 2.2: Predicted geometries for the $\tilde{X}\,^1\Sigma^+$ state of AlAlO at seven levels of sophistication with the four basis sets. Bond lengths are in Å.

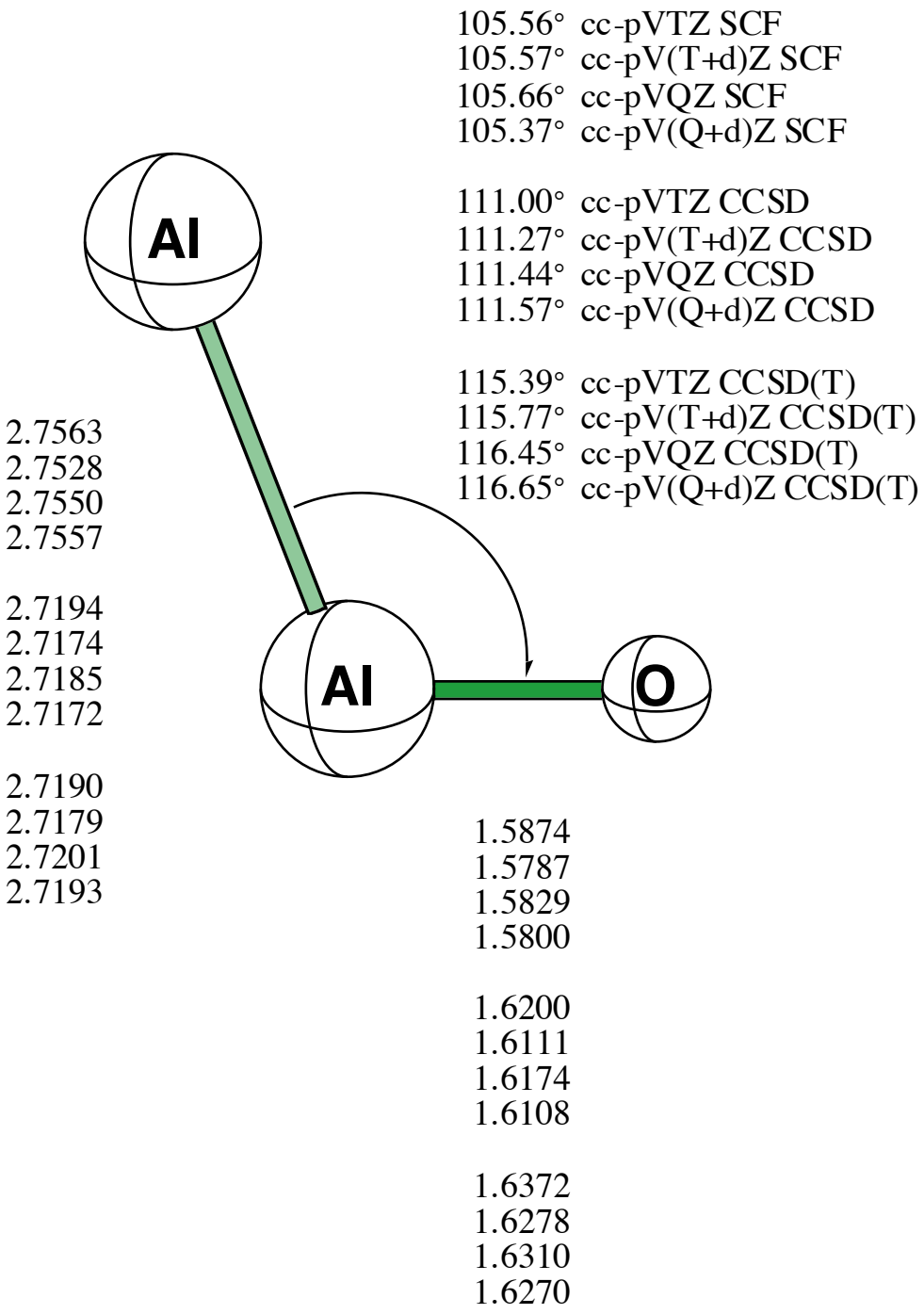

Figure 2.3: Predicted geometries of the transition state for the AlOAl↔AlAlO isomerization reaction. Bond lengths are in Å.

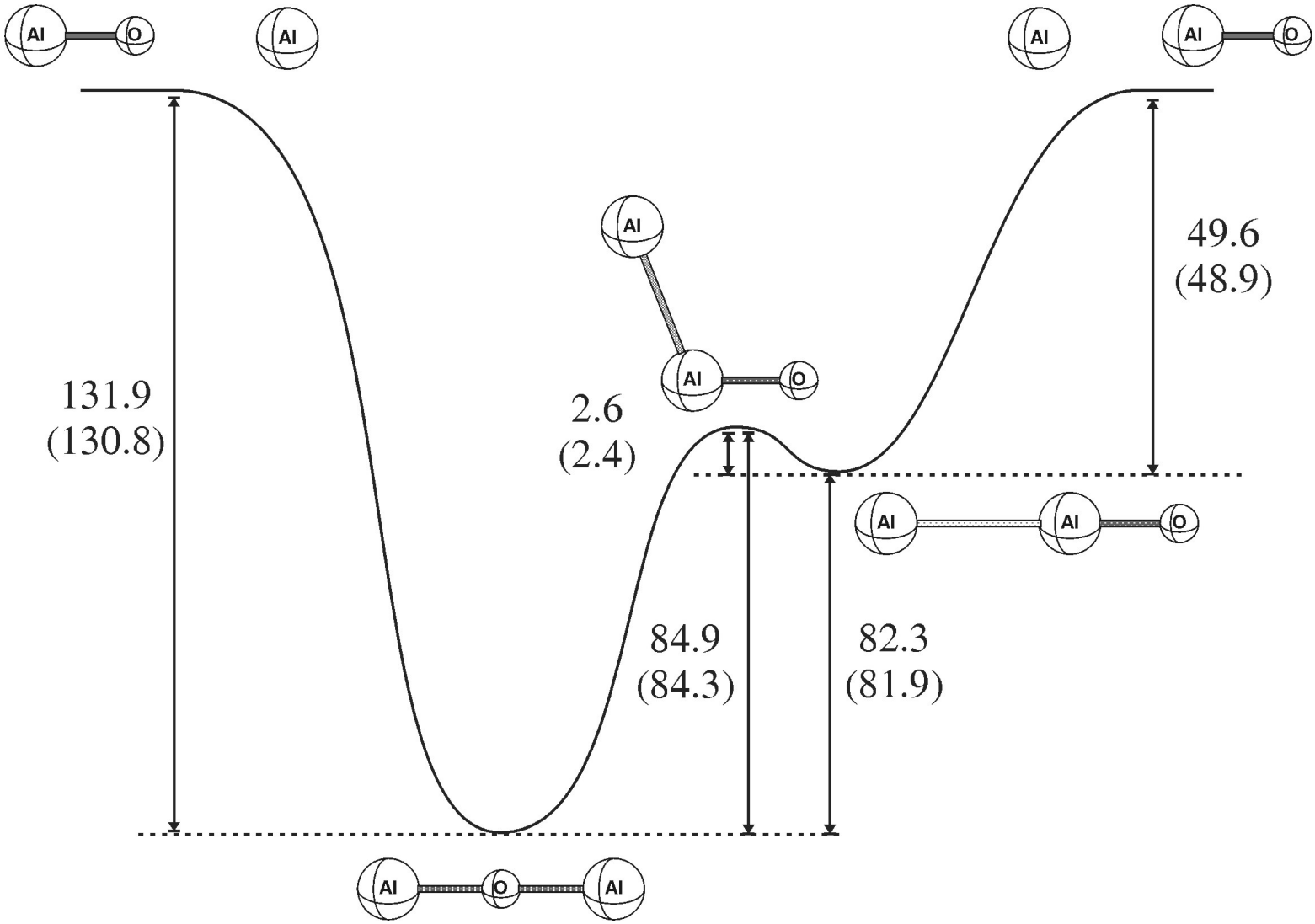

Figure 2.4: Schematic potential energy surface for the AlOAl - AlAlO system at the cc-pV(Q+d)Z CCSD(T) level of sophistication. Relative energies are reported in kcal mol^{-1} and ZPVE corrected values in parentheses.

CHAPTER 3

THE NEARLY DEGENERATE TRIPLET ELECTRONIC GROUND STATE ISOMERS OF LITHIUM NITROXIDE[†]

[†] Justin M. Turney and Henry F. Schaefer, III, submitted to *J. Phys. Chem. A* (2006).

3.1 ABSTRACT

The triplet electronic ground state potential energy surface of lithium nitroxide has been systematically investigated using convergent quantum mechanical methods. Equilibrium structures and physical properties for five stationary points (three minima and two transition states) have been determined employing highly correlated coupled cluster theory with four correlation-consistent polarized-valence (cc-pVXZ and aug-cc-pVXZ, X=T and Q) basis sets. The global minimum, roughly L-shaped Li-O-N, is predicted to lie 6.45 kcal mol^{-1} below the linear LiON minimum and 2.42 kcal mol^{-1} below the linear LiNO minimum. The barrier to isomerization from the global minimum to LiON was found to be 7.35 kcal mol^{-1} and with regard to LiNO 6.92 kcal mol^{-1}. The dissociation energies, D_0, with respect to Li + NO, have been predicted for all minima and for the global minimum was found to be 34.85 kcal mol^{-1}.

3.2 INTRODUCTION

Lithium nitroxide, a system that has only been studied a limited number of times over the past five decades, was first prepared in 1957 by Asmussen.[106] The first infrared (IR) study was by Andrews and Pimentel[107] in 1966 using argon matrix isolation techniques. They performed isotopic substitutions at all atomic positions to verify the molecular identity and to conduct a normal-coordinate analysis. Their vibrational frequencies were reported as ν_1 = 1352 cm^{-1}, ν_2 = 333 cm^{-1}, and ν_3 = 650.4 cm^{-1}. From their normal coordinate analysis they deduced a Li-O-N bond angle of 100 ± 10°, an ON bond length of 1.30 ± 0.05 Å, a LiO bond length of 1.63 Å, and a LiN bond length of 1.66 Å.

Then in 1971, Peslak, Klett, and David[108] published the first *ab initio* study on lithium nitroxide. Using a basis set consisting of six *s*-type Gaussians on lithium and 6*s* + 3*p* Gaussians on both nitrogen and oxygen they were able to predict a bent structure. The structure they arrived at was in good agreement with respect to bond distances but their bond angle falls 9 degrees below the lower bound given by Andrews and Pimentel[107] earlier. They assumed that the LiON system is closed-shell singlet but considered the possibility of it being a triplet. Their results suggested that this is the actual case, that Li(NO) is ionic, and it would contain the anion NO^- as an approximately identifiable moiety. At that time there was an experimental study by Asmussen[106] that supported their closed shell proposal that reporting Li(NO) as diamagnetic.

In 1973 Tevault and Andrews[109] reexamined the LiON matrix IR spectrum and provided evidence for photoisomerism. Tevault and Andrews report vibrational frequencies of 1352 and 651 cm^{-1} for a triangular LiON species. They also explain that during mercury photolysis the 651 cm^{-1} vibration observed disappears and a new 447 cm^{-1} appears, while the 1352 cm^{-1} slightly increases, suggesting that the triangular isomer photoisomerized to a bent form.

Girard-Dussau, Dargelos, and Chaillet[110] in 1982 used the CIPSI method with a 5-21G basis set. Their analysis is given assuming singlet and triplet ground states. It should be noted that the results given by Girard-Dussau *et. al.* for the triplet state do not show a triangular LiON minimum. They conclude that for the triplet system a linear LiON is the global minimum, linear LiNO is a local minimum, and a transition state with a LiON bond angle of about 30 degrees. They also made it known that for the singlet ground state a single determinant method will not accurately describe the system.

A second-order Møller-Plesset (MP2) study was performed by Spoliti, Damondo, Diomedi-Camassei, and Bencivenni[111] on three minima found on the triplet ground state potential energy surface. The reported geometry at their best level of theory (6-311+G* MP2) is r_{LiO} = 2.759 Å, r_{LiN} = 1.9035 Å, r_{ON} = 1.253 Å, and a bond angle of 120.5°.

A more recent study of the LiON system was performed by Vayner and Ball in 2001.[112] Singlet and triplet ground states for LiON were reported with a 6-311+G(d) basis set at the MP2 level of theory. This system has a π^2 highest occupied molecular orbital (HOMO) for which the lowest singlet electronic state requires a two-determinant reference function. On the other hand, the triplet can be described by a single determinant.

From the previous theoretical studies it may be seen that both electron correlation and a sufficient basis set is needed to qualitatively describe this system. In the present study the triplet electronic ground states of the linear ($\tilde{X}\,^3\Sigma^-$) and bent ($\tilde{X}\,^3A''$) LiON and the linear ($\tilde{X}\,^3\Sigma^-$) LiNO isomer of lithium nitroxide have been systematically studied using highly correlated methods available in our laboratory. Special emphasis is placed on the accurate determination of the relative energies for the isomerization between the three minima and dissociation energies for the three isomers into Li ($X\,^2S$) atom plus diatomic NO ($X\,^2P_{1/2}$) with high levels of theory up to single, double, and perturbative triple excitations coupled cluster theory.

3.3 THEORETICAL METHODS

Four basis sets were employed in order to optimize structures and determine physical properties of linear and bent LiON and linear LiNO as well as diatomic NO. The basis

sets were the correlation-consistent polarized-valence basis sets developed by Dunning and coworkers:[83] cc-pVXZ and aug-cc-pVXZ (X = T,Q). The larger augmented cc-pVXZ sets, designated by aug-cc-pVXZ, include diffuse functions. These were only employed for the oxygen and nitrogen atoms. The largest basis set aug-cc-pVQZ consists of 215 contracted Gaussian functions for the lithium nitroxide structures. Geometries were optimized with each basis set and level of theory. Harmonic vibrational frequencies were evaluated using analytic methods where available, and otherwise determined through finite differences of analytic gradients or numerical differentiation of total energies.

The electron configuration of the ground state ($X\ ^2\Pi_{1/2}$) of diatomic NO may be described as

$$[\text{core}](3\sigma)^2(4\sigma)^2(5\sigma)^2(1\pi)^4(2\pi) \qquad X\ ^2\Pi_{1/2} \qquad (3.1)$$

where [core] designates the two core (O—1*s*-like and N—1*s*-like) orbitals. For $\tilde{X}\ ^3\Sigma^-$ LiON and LiNO the ground state electron configuration may be described with

$$[\text{core}](4\sigma)^2(5\sigma)^2(6\sigma)^2(1\pi)^4(2\pi)^2 \qquad \tilde{X}\ ^3\Sigma^- \qquad (3.2)$$

where [core] designates the three core (Li—1*s*-like, O—1*s*-like and N—1*s*-like) orbitals. Finally, for $\tilde{X}\ ^3A''$ LiON the electron configuration is

$$[\text{core}](4a')^2(5a')^2(1a')^2(1a'')^2(7a')^2(8a')^2(2a'')^2 \qquad \tilde{X}\ ^3A'' \qquad (3.3)$$

The zeroth-order descriptions for all species were obtained using single configuration SCF [restricted open-shell Hartree-Fock (ROHF)] wave function. Correlation effects were included using configuration interaction with single and double excitations (CISD), coupled cluster with single and double excitations (CCSD),[35,83,89] and CCSD with perturbative triples [CCSD(T)][90,91] levels of theory. In the correlated

procedures the two core orbitals were frozen for ON and three core orbitals were frozen for LiON. The MOLPRO[95,97,113] *ab initio* program package was utilized during this study.

3.4 RESULTS AND DISCUSSION

In Table 3.1 total energies and physical properties for the $X\,^2\Pi_{1/2}$ state of diatomic NO are presented. In Figures 3.1 and 3.2 the optimized geometries for $\tilde{X}\,^3\Sigma^-$ LiON and LiNO are depicted at four levels of sophistication with four basis sets. Total energies and physical properties of these two structures are presented in Tables 3.2 and 3.3. Figure 3.3 provides the optimized geometries for the $\tilde{X}\,^3A''$ minimum of LiON. Total energies and physical properties for this structure are presented in Table 3.4. Provided in Figures 3.4 and 3.5 are the optimized geometries for the transition states found on this potential energy surface. The total energies and physical properties for these transition states can be found in Table 3.5 and 3.6. Energies relative to the $\tilde{X}\,^3A''$ global minimum for all other geometries are found in Table 3.7. Barrier heights for isomerization of the linear $\tilde{X}\,^3\Sigma^-$ LiON and LiNO structures to the bent minimum are located in Table 3.8. A pictorial representation of the potential energy surface of this system is found in Figure 3.6.

3.4.1 Geometries

The equilibrium bond length for the ground state ($X\,^2\Pi_{1/2}$) of diatomic NO is experimentally determined to be r_e(ON) = 1.15077 Å[61] and is in reasonable agreement with the predicted bond length of 1.1530 Å. The theoretically predicted NO bond length generally increases with advanced treatments of correlation effects and decreases with

larger basis sets. The inclusion of the diffuse function on both atoms shortens the ON bond distance at all levels of theory.

For the local minimum linear LiON isomer, including electron correlation through coupled cluster methods yields a general trend of increasing LiO and ON bond lengths (Figure 3.1). These bond lengths are shortened with increasing basis set size. The inclusion of the diffuse functions on N and O increases the bond lengths. A previous theoretical study[112] predicted r_e(LiO) = 1.648 Å and r_e(NO) = 1.274 Å with the 6-311+G(d) MP2 method compared to the present study, in which r_e(LiO) = 1.6387 Å and r_e(NO) = 1.2739 Å aug-cc-pVQZ CCSD(T).

The linear LiNO isomer follows a similar trend as that for linear LiON. Advanced treatments of electron correlation yield an elongation of both LiN and NO bond lengths (Figure 3.2). The bond lengths contract with increasing basis set, but inclusion of diffuse functions lengthen the bonds. For linear LiNO Vayner and Ball[112] predicted r_e(LiN) = 1.724 Å and r_e(ON) = 1.223 Å with 6-311+G(d) MP2 compared to the present results, r_e(LiN) = 1.7289 Å and r_e(ON) = 1.2202 Å with aug-cc-pVQZ CCSD(T). The NO bond length in LiNO is elongated as well, though not as much as in LiON.

The bent global minimum $\tilde{X}\,^3A''$ LiON structures are shown in Figure 3.3. With inclusion of electron correlation the LiO and ON bond lengths increase, while the LiON angle decreases by ~6°. The $\tilde{X}\,^3A''$ LiO bond distance is longer (by 1.813 – 1.639 = 0.174 Å) than that for linear LiON. As for the $\tilde{X}\,^3A''$ ON equilibrium separation, compared to linear Li-ON, this bond distance is reasonably consistent. However for linear Li-NO the NO distance is significantly longer (1.275 – 1.220 = 0.055 Å) than for the $\tilde{X}\,^3A''$ state. When compared to the previous theoretical work[112] [r_e(LiO) = 1.841 Å, r_e(ON) = 1.271

Å, and α_e(LiON) = 72° with 6-311+G(d) MP2] the present results are qualitatively consistent [r_e(LiO) = 1.813 Å, r_e(ON) = 1.275 Å, and α_e(LiON) = 73.6° with aug-cc-pVQZ CCSD(T)].

Figure 3.4 shows the transition state structure for isomerization between $\tilde{X}\,^3A''$ LiON and $\tilde{X}\,^3\Sigma^-$ LiON (denoted as LiON TS). Figure 3.5 reports the transition state structure between $\tilde{X}\,^3A''$ LiON and $\tilde{X}\,^3\Sigma^-$ LiON (denoted as LiNO TS) at four levels of theoretical sophistication with four basis sets. The LiON TS has a bond angle of 130°, which is closer to the linear LiON structure. This feature is consistent with the Hammond postulate,[101] which states that the transition state should have a structure closer to that of the reactant for an exothermic process. In regard to the LiNO TS the Hammond postulate is not valid because the LiNO transition state is closer to triangular LiON.

The inclusion of the 1*s* core electrons on lithium results in a shortening of the Li-X (X = O, N) bond lengths for all conformations at the correlated levels. This effect can be surprisingly large, as may be seen for the $\tilde{X}\,^3A''$ state by comparing the Li-N distance [cc-pVQZ CCSD(T) value 1.809 Å] without core correlation to the value 1.793 predicted with the cc-pCVQZ CCSD(T) method. The bond angles found in the bent minimum and transition states do not show significant changes with the use of the core-correlated basis sets.

3.4.2 Harmonic Vibrational Frequencies

The harmonic vibrational frequency for the $X\,^2\Pi_{1/2}$ ground state of diatomic NO has been experimentally determined[61] to be 1904 cm^{-1}. The vibrational frequencies from the coupled cluster methods are in good agreement with the experimental values, e.g., ω_e =

1907 for the aug-cc-pVQZ CCSD(T) method. Advanced treatments of electron correlation result in a decrease in the stretching frequency.

The three harmonic vibrational frequencies for the $\tilde{X}\,^3\Sigma^-$ LiON system are also predicted to be lowered with the correlated wave functions relative to those with the SCF method, reflecting the longer LiO and ON bond lengths with correlated methods. The three correlated methods employed [CISD, CCSD, and CCSD(T)] present very similar vibrational frequencies. The predicted frequencies for the linear Li-ON structure at the aug-cc-pVQZ CCSD(T) level of theory (Table 3.2) are ω_1 = 1408 cm^{-1}, ω_2 = 140 cm^{-1}, and ω_3 = 763 cm^{-1}.

For the $\tilde{X}\,^3\Sigma^-$ Li-NO structure the three harmonic vibrational frequencies are predicted to decrease with the correlated wave functions relative to the SCF results as well. This decrease reflects the longer LiN and NO bond distances with the correlated methods. The predicted frequencies for the linear Li-NO structure at the aug-cc-pVQZ CCSD(T) level of theory are ω_1 = 1646 cm^{-1}, ω_2 = 205 cm^{-1}, and ω_3 = 715 cm^{-1}.

The harmonic vibrational frequencies for the $\tilde{X}\,^3A''$ LiON global minimum at the aug-cc-pVQZ CCSD(T) level of theory (in Table 3.4) are ω_1 = 1375 cm^{-1}, ω_2 = 367 cm^{-1}, and ω_3 = 681 cm^{-1}. These compare well with the 1966 Andrews-Pimentel[107] experimental values ν_1 = 1352 cm^{-1}, ν_2 = 333 cm^{-1}, and ν_3 = 650 cm^{-1}, or the more recent Andrews, Zhou, and Wang[114] experimental values of ν_1 = 1351 cm^{-1} and ν_3 = 651 cm^{-1}. All vibrational frequencies decrease with the advanced treatments of electron correlation. The $\tilde{X}$ NO $^3A''$ stretching frequency (1351 cm^{-1}) shows a significant reduction relative to that of diatomic NO (1907 cm^{-1}) and is slightly smaller than that predicted for linear

LiON (1408 cm^{-1}). This feature is consistent with Badger's rule,[102,103] that the larger force constant (high vibrational frequency) may be associated with the shorter bond length.

Harmonic vibrational frequencies for the LiON transition state are provided in Table 3.5. The predicted frequencies at the aug-cc-pVQZ CCSD(T) level of theory are ω_1 = 1356 cm^{-1}, ω_2 = 171*i* cm^{-1}, and ω_3 = 752 cm^{-1}. The LiO stretching frequency ω_1 for the transition state is lower than that for the linear LiON molecule, reflecting the longer bond distance.

The LiNO transition state harmonic vibrational frequencies are presented in Table 3.6. The predicted frequencies at the aug-cc-pVQZ CCSD(T) level of theory are ω_1 = 1497 cm^{-1}, ω_2 = 230*i* cm^{-1}, and ω_3 = 701 cm^{-1}. The lower LiN stretching ω_3 frequency for this transition state lies below that for the linear LiNO molecule, reflecting the longer LiN bond length.

3.4.3 Energetics

Relative energies between the ground states of the three lithium nitroxide isomers are given in Table 3.7. With the aug-cc-pVQZ basis set the classical relative energies T_e for the linear LiON with respect to the bent global minimum LiON are predicted to be [at the aug-cc-pVQZ CCSD(T)] level of theory 6.4 kcal mol^{-1}; for the LiON transition state 7.8 kcal mol^{-1}; for linear LiNO 1.9 kcal mol^{-1}; for the LiNO transition state 7.2 kcal mol^{-1}. The energy separation generally increases for Li-ON and the LiON transition state but decreases the Li-NO and for the LiNO transition state with advance treatments of electron correlation. The inclusion of zero-point vibrational energy (ZPVE) lowers the relative energy for the linear minima and raises it for the transition states. Compared to a

previous theoretical study[112] our relative energies are higher for the secondary minima [previous work: linear LiON 6.2 kcal mol^{-1} and linear LiNO 0.8 kcal mol^{-1} 6-311+G(d) MP2]. With the consideration of the core-correlated basis sets, the changes in relative energies are all less than 0.35 kcal mol^{-1}. The largest relative energy change occurs for the Li-NO transition state. This stationary point (TS2) lies 7.58 kcal above the $\tilde{X}\,^3A''$ global minimum with cc-pVQZ CCSD(T), but at 7.93 kcal with cc-pCVQZ CCSD(T).

The ZPVE corrected barrier heights for the isomerization reaction

$$\text{linear LiON} \leftarrow \text{LiON TS} \leftarrow \text{triangular LiON} \rightarrow \text{LiNO TS} \rightarrow \text{linear LiNO}$$

are presented in Figure 3.6 at the cc-pVQZ CCSD(T) level of sophistication. The activation energy for the reaction $\text{triangular LiON} \rightarrow \text{LiON TS}$ is predicted to be 8.01 kcal mol^{-1} and for $\text{triangular LiON} \rightarrow \text{LiNO TS}$ 7.25 kcal mol^{-1}. For the reverse reaction back to triangular LiON the activation energy is 0.90 kcal mol^{-1} for linear LiON and 4.50 kcal mol^{-1} for linear LiNO.

Dissociation energies for the formation of Li and ON are provided in Table 3.8. For the roughly L-shaped isomer the energy to dissociation is 34.9 kcal mol^{-1}, linear LiON is 28.4 kcal mol^{-1}, and for linear LiNO it is 32.4 kcal mol^{-1}. The inclusion of electron correlation increases the dissociation energy by about 10 kcal mol^{-1} for each isomer. With larger basis sets the dissociation energies also increase. Inclusion of lithium 1*s* core-correlation does not meaningfully alter the dissociation energy, as seen in Table 3.8. Dissociation into Li^+ and NO^- is a significantly higher energy process than into neutral Li and NO, and this ionic pathway not expected to be competitive in the gas phase, because the ionization potential of Li is much greater than the electron affinity of NO.

3.5 CONCLUSIONS

The triplet electronic ground state isomers ($\tilde{X}\,^3\Sigma^-$ and $\tilde{X}\,^3A''$ LiON, and $\tilde{X}\,^3\Sigma^-$ LiNO) of lithium nitroxide have been studied using convergent quantum mechanical methods. It was demonstrated that the global minimum is the approximately L-shaped Li-O-N structure at coupled cluster levels of theory. At the aug-cc-pVQZ CCSD(T) level the $\tilde{X}\,^3A''$ state of LiON is predicted to have the following harmonic vibrational frequencies ω_1 = 1375 cm^{-1}, ω_2 = 367 cm^{-1}, and ω_3 = 681 cm^{-1}, which compare well to the Andrews and Pimentel's experimental fundamental frequencies[107] ν_1 = 1352 cm^{-1}, ν_2 = 333 cm^{-1}, and ν_3 = 650 cm^{-1}, respectively. Triangular (roughly L-shaped) LiON is predicted to lie 6.5 kcal mol^{-1} below linear LiON and 2.4 kcal mol^{-1} below linear LiNO. The dissociation energy to Li + NO is predicted to be 34.9 kcal mol^{-1} for triangular LiON, 28.4 kcal mol^{-1} for linear LiON, and 32.4 kcal mol^{-1} for linear LiNO. Although LiON is an ionic system consideration of the core effects of lithium does not significantly change the predictions reported here.

3.6 ACKNOWLEDGEMENTS

This research was supported by the U.S. National Science Foundation, Grant No. CHE-0451445. The authors would like to thank Dr. Yukio Yamaguchi for useful discussions.

Table 3.1: Total energies (in hartree), dipole moments (in debye), harmonic vibrational frequencies (in cm^{-1}), infrared (IR) intensities (in km mol^{-1}), and ZPVE (in kcal mol^{-1}) for the ground state ($X\ ^2\Pi_{1/2}$) of NO.

Level of Theory	Total energy	r_e (NO)	μ_e	ω_e	ZPVE
cc-pVTZ SCF	-129.292 158	1.1141	0.155	2253 (92)	3.22
aug-cc-pVTZ SCF	-129.293 780	1.1139	0.135	2241 (96)	3.20
cc-pVQZ SCF	-129.301 897	1.1125	0.141	2248 (93)	3.21
aug-cc-pVQZ SCF	-129.302 494	1.1125	0.129	2246 (95)	3.21
cc-pVTZ CASSCF	-129.409 406	1.1587			
aug-cc-pVTZ CASSCF	-129.410 768	1.1588			
cc-pVQZ CASSCF	-129.418 862	1.1570			
aug-cc-pVQZ CASSCF	-129.419 361	1.1570			
cc-pVTZ CISD	-129.669 284	1.1373		2076	2.97
aug-cc-pVTZ CISD	-129.676 587	1.1370		2067	2.95
cc-pVQZ CISD	-129.703 066	1.1333		2088	2.98
aug-cc-pVQZ CISD	-129.706 060	1.1330		2085	2.98
cc-pVTZ CCSD	-129.697 891	1.1471		1986	2.84
aug-cc-pVTZ CCSD	-129.706 304	1.1471		1975	2.82
cc-pVQZ CCSD	-129.733 655	1.1432		1996	2.85
aug-cc-pVQZ CCSD	-129.736 995	1.1433		1993	2.85
cc-pVTZ CCSD(T)	-129.717 072	1.1565		1902	2.72
aug-cc-pVTZ CCSD(T)	-129.726 367	1.1569		1889	2.70
cc-pVQZ CCSD(T)	-129.754 601	1.1528		1911	2.73
aug-cc-pVQZ CCSD(T)	-129.758 316	1.1530		1907	2.73
Experiment[a]		1.1508		1904	
Experiment[b]			0.16		

[a] Reference 61
[b] Reference 115

Table 3.2: Total energies (in hartree), dipole moments (in debye), harmonic vibrational frequencies (in cm^{-1}), infrared (IR) intensities (in km mol^{-1}), and zero-point vibrational energies (ZPVE) (in kcal mol^{-1}) for the linear equilibrium geometry ($\tilde{X}\ ^3\Sigma^-$ state) of LiON. IR intensities of the ω_2 mode were doubled.

Level of Theory	Total energy	μ_e	$\omega_1(\sigma^+)$	$\omega_2(\pi)$	$\omega_3(\sigma^+)$	ZPVE
cc-pVTZ SCF	-136.763 310	7.627	1495 (300)	150 (105)	817 (130)	3.73
aug-cc-pVTZ SCF	-136.765 460	7.730	1488 (322)	148 (105)	814 (135)	3.71
cc-pCVTZ SCF	-136.763 703	7.605	1495 (299)	150 (106)	817 (129)	3.73
cc-pVQZ SCF	-136.773 613	7.664	1495 (305)	150 (106)	822 (132)	3.74
aug-cc-pVQZ SCF	-136.774 128	7.714	1494 (320)	147 (104)	820 (135)	3.73
cc-pCVQZ SCF	-136.773 716	7.660	1495 (305)	150 (106)	823 (132)	3.74
cc-pVTZ CASSCF	-136.928 995					
aug-cc-pVTZ CASSCF	-136.931 354					
cc-pVQZ CASSCF	-136.939 992					
aug-cc-pVQZ CASSCF	-136.940 506					
cc-pVTZ CISD	-137.143 504		1472	147	793	3.66
aug-cc-pVTZ CISD	-137.152 709		1465	141	784	3.62
cc-pCVTZ CISD	-137.181 366		1475	151	798	3.68
cc-pVQZ CISD	-137.179 402		1484	146	797	3.68
aug-cc-pVQZ CISD	-137.182 998		1482	141	791	3.65
cc-pCVQZ CISD	-137.219 009		1488	151	807	3.74
cc-pVTZ CCSD	-137.175 325		1430	149	781	3.59
aug-cc-pVTZ CCSD	-137.186 095		1423	142	768	3.54
cc-pCVTZ CCSD	-137.217 993		1430	153	785	3.60
cc-pVQZ CCSD	-137.213 596		1443	147	783	3.60
aug-cc-pVQZ CCSD	-137.217 769		1440	143	776	3.58
cc-pCVQZ CCSD	-137.258 330		1443	153	792	3.63
cc-pVTZ CCSD(T)	-137.192 206		1401	147	772	3.53
aug-cc-pVTZ CCSD(T)	-137.204 431		1391	140	756	3.47
cc-pCVTZ CCSD(T)	-137.235 020		1400	151	777	3.54
cc-pVQZ CCSD(T)	-137.232 775		1411	144	772	3.53
aug-cc-pVQZ CCSD(T)	-137.237 497		1408	140	763	3.50
cc-pCVQZ CCSD(T)	-137.277 686		1412	150	782	3.56

Table 3.3: Total energies (in hartree), dipole moments (in debye), harmonic vibrational frequencies (in cm^{-1}), infrared (IR) intensities (in km mol^{-1}), and zero-point vibrational energies (ZPVE) (in kcal mol^{-1}) for the linear equilibrium geometry ($\tilde{X}\ ^3\Sigma^-$ state) of LiNO. IR intensities of the ω_2 mode were doubled.

Level of Theory	Total energy	μ_e	$\omega_1(\sigma^+)$	$\omega_2(\pi)$	$\omega_3(\sigma^+)$	ZPVE
cc-pVTZ SCF	-136.751 623	7.710	1913 (180)	231 (77)	745 (223)	4.46
aug-cc-pVTZ SCF	-136.754 177	7.877	1896 (191)	225 (80)	741 (235)	4.41
cc-pCVTZ SCF	-136.751 912	7.699	1913 (179)	230 (78)	746 (222)	4.46
cc-pVQZ SCF	-136.761 955	7.777	1906 (188)	228 (81)	747 (230)	4.44
aug-cc-pVQZ SCF	-136.762 747	7.850	1901 (192)	226 (80)	744 (235)	4.43
cc-pCVQZ SCF	-136.762 028	7.774	1906 (188)	228 (81)	745 (229)	4.44
cc-pVTZ CASSCF	-136.919 526					
aug-cc-pVTZ CASSCF	-136.923 301					
cc-pVQZ CASSCF	-136.931 332					
aug-cc-pVQZ CASSCF	-136.932 405					
cc-pVTZ CISD	-137.146 275		1795	222	740	4.26
aug-cc-pVTZ CISD	-137.155 892		1784	213	732	4.21
cc-pCVTZ CISD	-137.183 914		1803	226	746	4.29
cc-pVQZ CISD	-137.182 488		1802	218	741	4.26
aug-cc-pVQZ CISD	-137.186 256		1799	215	737	4.24
cc-pCVQZ CISD	-137.221 908		1811	224	750	4.30
cc-pVTZ CCSD	-137.179 954		1707	212	727	4.09
aug-cc-pVTZ CCSD	-137.190 938		1691	205	716	4.03
cc-pCVTZ CCSD	-137.222 537		1710	217	733	4.11
cc-pVQZ CCSD	-137.218 443		1713	211	727	4.09
aug-cc-pVQZ CCSD	-137.222 655		1707	207	722	4.06
cc-pCVQZ CCSD	-137.263 135		1717	216	735	4.12
cc-pVTZ CCSD(T)	-137.199 110		1650	211	722	4.00
aug-cc-pVTZ CCSD(T)	-137.211 508		1631	203	709	3.93
cc-pCVTZ CCSD(T)	-137.241 859		1653	215	729	4.02
cc-pVQZ CCSD(T)	-137.239 914		1653	209	721	3.99
aug-cc-pVQZ CCSD(T)	-137.244 664		1646	205	715	3.96
cc-pCVQZ CCSD(T)	-137.284 802		1657	215	730	4.02

Table 3.4: Total energies (in hartree), dipole moments (in debye), harmonic vibrational frequencies (in cm^{-1}), infrared (IR) intensities (in km mol^{-1}), and zero-point vibrational energies (ZPVE) (in kcal mol^{-1}) for the bent equilibrium geometry ($\tilde{X}\ ^3A''$ state) of LiON.

Level of Theory	Total energy	μ_e	$\omega_1(a')$	$\omega_2(a')$	$\omega_3(a')$	ZPVE
cc-pVTZ SCF	-136.761 790	6.368	1490 (214)	323 (34)	743 (151)	3.65
aug-cc-pVTZ SCF	-136.764 080	6.429	1484 (222)	320 (35)	738 (154)	3.63
cc-pCVTZ SCF	-136.762 113	6.354	1489 (214)	322 (34)	742 (149)	3.65
cc-pVQZ SCF	-136.772 113	6.376	1490 (217)	323 (35)	747 (149)	3.66
aug-cc-pVQZ SCF	-136.772 715	6.411	1489 (222)	321 (36)	744 (153)	3.65
cc-pCVQZ SCF	-136.772 213	6.375	1490 (217)	323 (35)	747 (150)	3.66
cc-pVTZ CASSCF	-136.935 560					
aug-cc-pVTZ CASSCF	-136.937 977					
cc-pVQZ CASSCF	-136.946 536					
aug-cc-pVQZ CASSCF	-136.947 118					
cc-pVTZ CISD	-137.150 428		1493	372	705	3.67
aug-cc-pVTZ CISD	-137.159 462		1488	367	696	3.65
cc-pCVTZ CISD	-137.188 166		1498	377	710	3.70
cc-pVQZ CISD	-137.186 224		1507	372	707	3.70
aug-cc-pVQZ CISD	-137.189 754		1505	368	703	3.68
cc-pCVQZ CISD	-137.225 771		1512	378	716	3.72
cc-pVTZ CCSD	-137.184 533		1408	373	695	3.54
aug-cc-pVTZ CCSD	-137.194 772		1402	365	683	3.50
cc-pCVTZ CCSD	-137.227 272		1407	380	700	3.55
cc-pVQZ CCSD	-137.222 489		1422	373	696	3.56
aug-cc-pVQZ CCSD	-137.226 432		1420	368	690	3.66
cc-pCVQZ CCSD	-137.267 340		1421	381	705	3.58
cc-pVTZ CCSD(T)	-137.203 196		1366	373	688	3.47
aug-cc-pVTZ CCSD(T)	-137.214 633		1358	364	674	3.53
cc-pCVTZ CCSD(T)	-137.246 136		1365	381	694	3.49
cc-pVQZ CCSD(T)	-137.243 342		1377	373	688	3.49
aug-cc-pVQZ CCSD(T)	-137.247 724		1375	367	681	3.46
cc-pCVQZ CCSD(T)	-137.288 408		1377	381	697	3.51
Experimental[a]			1352	333	650.4	
Experimental[b]			1352		651	
Experimental[c]			1351		651	
Experimental[d]			1351.0		651.7	

[a] Reference 107

[b] Reference 109

[c] Reference 114

[d] Reference 116

Table 3.5: Total energies (in hartree), dipole moments (in debye), harmonic vibrational frequencies (in cm^{-1}), infrared (IR) intensities (in km mol^{-1}), and zero-point vibrational energies (ZPVE) (in kcal mol^{-1}) for the isomerization transition state ($\tilde{X}\ ^3A''$) of LiON.

Level of Theory	Total energy	μ_e	$\omega_1(a')$	$\omega_2(a')$	$\omega_3(a')$	ZPVE
cc-pVTZ SCF	-136.758 555	7.438	1423 (220)	182*i*	808 (153)	3.19
aug-cc-pVTZ SCF	-136.760 929	7.511	1419 (235)	179*i*	802 (156)	3.17
cc-pCVTZ SCF	-136.758 932	7.415	1423 (219)	183*i*	807 (152)	3.19
cc-pVQZ SCF	-136.768 924	7.450	1425 (224)	182*i*	811 (153)	3.20
aug-cc-pVQZ SCF	-136.769 603	7.487	1425 (235)	180*i*	808 (156)	3.19
cc-pCVQZ SCF	-136.769 036	7.446	1425 (224)	182*i*	811 (153)	3.20
cc-pVTZ CASSCF	-136.927 013					
aug-cc-pVTZ CASSCF	-136.929 602					
cc-pVQZ CASSCF	-136.938 131					
aug-cc-pVQZ CASSCF	-136.938 813					
cc-pVTZ CISD	-137.140 498		1418	178*i*	780	3.14
aug-cc-pVTZ CISD	-137.149 964		1413	173*i*	768	3.12
cc-pCVTZ CISD	-137.178 156		1431	174*i*	776	3.16
cc-pVQZ CISD	-137.176 447		1432	178*i*	781	3.16
aug-cc-pVQZ CISD	-137.180 224		1431	174*i*	776	3.16
cc-pCVQZ CISD	-137.215 853		1436	183*i*	791	3.18
cc-pVTZ CCSD	-137.172 720		1377	178*i*	769	3.07
aug-cc-pVTZ CCSD	-137.183 728		1370	170*i*	754	3.04
cc-pCVTZ CCSD	-137.215 208		1375	182*i*	773	3.07
cc-pVQZ CCSD	-137.211 040		1390	176*i*	769	3.09
aug-cc-pVQZ CCSD	-137.215 373		1388	172*i*	762	3.07
cc-pCVQZ CCSD	-137.255 576		1389	181*i*	778	3.10
cc-pVTZ CCSD(T)	-137.189 817		1348	178*i*	762	3.02
aug-cc-pVTZ CCSD(T)	-137.202 256		1339	169*i*	744	2.98
cc-pCVTZ CCSD(T)	-137.232 471		1346	182*i*	767	3.02
cc-pVQZ CCSD(T)	-137.230 430		1359	176*i*	760	3.03
aug-cc-pVQZ CCSD(T)	-137.234 293		1356	171*i*	752	3.01
cc-pCVQZ CCSD(T)	-137.275 144		1357	182*i*	770	3.04

Table 3.6: Total energies (in hartree), dipole moments (in debye), harmonic vibrational frequencies (in cm^{-1}), infrared (IR) intensities (in km mol^{-1}), and zero-point vibrational energies (ZPVE) (in kcal mol^{-1}) for the isomerization transition state ($\tilde{X}\ ^3A''$) of LiNO.

Level of Theory	Total energy	μ_e	$\omega_1(a')$	$\omega_2(a')$	$\omega_3(a')$	ZPVE
cc-pVTZ SCF	-136.742 444	7.887	1753 (156)	257*i*	722 (152)	3.54
aug-cc-pVTZ SCF	-136.745 264	8.000	1738 (170)	253*i*	716 (155)	3.51
cc-pCVTZ SCF	-136.742 729	7.870	1753 (155)	256*i*	722 (151)	3.54
cc-pVQZ SCF	-136.752 829	7.918	1746 (164)	256*i*	722 (151)	3.53
aug-cc-pVQZ SCF	-136.753 714	7.976	1742 (169)	254*i*	718 (154)	3.52
cc-pCVQZ SCF	-136.752 899	7.918	1746 (164)	256*i*	722 (151)	3.53
cc-pVTZ CASSCF	-136.917 143					
aug-cc-pVTZ CASSCF	-136.920 779					
cc-pVQZ CASSCF	-136.928 755					
aug-cc-pVQZ CASSCF	-136.929 813					
cc-pVTZ CISD	-137.136 963		1658	245*i*	725	3.41
aug-cc-pVTZ CISD	-137.146 835		1647	241*i*	714	3.38
cc-pCVTZ CISD	-137.174 271		1666	250*i*	729	3.42
cc-pVQZ CISD	-137.173 096		1667	244*i*	724	3.42
aug-cc-pVQZ CISD	-137.177 028		1663	244*i*	719	3.40
cc-pCVQZ CISD	-137.212 135		1674	249*i*	732	3.44
cc-pVTZ CCSD	-137.171 294		1566	237*i*	714	3.25
aug-cc-pVTZ CCSD	-137.182 532		1548	234*i*	713	3.23
cc-pCVTZ CCSD	-137.213 568		1556	241*i*	719	3.25
cc-pVQZ CCSD	-137.209 696		1563	237*i*	713	3.25
aug-cc-pVQZ CCSD	-137.214 087		1557	234*i*	707	3.24
cc-pCVQZ CCSD	-137.254 019		1563	242*i*	721	3.27
cc-pVTZ CCSD(T)	-137.190 548		1500	234*i*	710	3.16
aug-cc-pVTZ CCSD(T)	-137.203 183		1482	228*i*	696	3.11
cc-pCVTZ CCSD(T)	-137.232 982		1500	238*i*	716	3.17
cc-pVQZ CCSD(T)	-137.231 264		1503	233*i*	708	3.16
aug-cc-pVQZ CCSD(T)	-137.236 182		1497	230*i*	701	3.14
cc-pCVQZ CCSD(T)	-137.275 771		1504	239*i*	717	3.17

Table 3.7: Relative energies of the (LiNO) structures with respect to the triangular global minimum, in kcal mol^{-1}, with zero-point vibrational energy corrected values in parentheses.

	Relative Energy				
Level of Theory	$\tilde{X}\ ^3\Sigma^-$ LiON	$\tilde{X}\ ^3A''$ TS1	$\tilde{X}\ ^3A''$ LiON	$\tilde{X}\ ^3A''$ TS2	$\tilde{X}\ ^3\Sigma^-$ LiNO
cc-pVTZ SCF	-0.95 (-0.87)	2.03 (1.57)	0.00	12.14 (12.03)	6.38 (7.19)
aug-cc-pVTZ SCF	-0.87 (-0.79)	1.98 (1.52)	0.00	11.81 (11.69)	6.21 (6.99)
cc-pCVTZ SCF	-1.00 (-0.92)	2.00 (1.53)	0.00	12.16 (12.05)	6.40 (7.21)
cc-pVQZ SCF	-0.94 (-0.86)	2.00 (1.54)	0.00	12.10 (11.97)	6.37 (7.15)
aug-cc-pVQZ SCF	-0.89 (-0.81)	1.95 (1.49)	0.00	11.92 (11.79)	6.26 (7.04)
cc-pCVQZ SCF	-0.94 (-0.86)	1.99 (1.53)	0.00	12.12 (11.99)	6.39 (7.17)
cc-pVTZ CISD	4.34 (4.33)	6.23 (5.70)	0.00	8.45 (8.19)	2.61 (3.20)
aug-cc-pVTZ CISD	4.24 (4.21)	5.96 (5.43)	0.00	7.92 (7.65)	2.24 (2.80)
cc-pCVTZ CISD	4.27 (4.25)	6.28 (5.74)	0.00	8.72 (8.45)	2.67 (3.26)
cc-pVQZ CISD	4.28 (4.26)	6.14 (5.60)	0.00	8.24 (7.96)	2.34 (2.90)
aug-cc-pVQZ CISD	4.24 (4.21)	5.98 (5.46)	0.00	7.99 (7.71)	2.20 (2.76)
cc-pCVQZ CISD	4.24 (4.23)	6.22 (5.68)	0.00	8.56 (8.27)	2.42 (3.00)
cc-pVTZ CCSD	5.78 (5.83)	7.41 (6.94)	0.00	8.31 (8.02)	2.87 (3.42)
aug-cc-pVTZ CCSD	5.44 (5.48)	6.93 (6.47)	0.00	7.68 (7.41)	2.41 (2.94)
cc-pCVTZ CCSD	5.82 (5.88)	7.57 (7.09)	0.00	8.60 (8.30)	2.97 (3.53)
cc-pVQZ CCSD	5.58 (5.62)	7.18 (6.71)	0.00	8.03 (7.72)	2.54 (3.07)
aug-cc-pVQZ CCSD	5.44 (5.36)	6.94 (6.35)	0.00	7.75 (7.33)	2.37 (2.77)
cc-pCVQZ CCSD	5.65 (5.71)	7.38 (6.90)	0.00	8.36 (8.05)	2.64 (3.18)
cc-pVTZ CCSD(T)	6.90 (6.96)	8.40 (7.95)	0.00	7.94 (7.63)	2.56 (3.09)
aug-cc-pVTZ CCSD(T)	6.40 (6.34)	7.77 (7.22)	0.00	7.18 (6.76)	1.96 (2.36)
cc-pCVTZ CCSD(T)	6.98 (7.03)	8.58 (8.11)	0.00	8.25 (7.93)	2.68 (3.21)
cc-pVQZ CCSD(T)	6.63 (6.67)	8.10 (7.64)	0.00	7.58 (7.25)	2.15 (2.65)
aug-cc-pVQZ CCSD(T)	6.42 (6.45)	7.80 (7.35)	0.00	7.24 (6.92)	1.92 (2.42)
cc-pCVQZ CCSD(T)	6.73 (6.78)	8.32 (7.85)	0.00	7.93 (7.60)	2.26 (2.77)

Table 3.8: Dissociation energies of linear and bent LiON and linear LiNO into atomic Li (^2S) plus NO ($X\ ^2\Pi_{1/2}$) in kcal mol^{-1}. Zero-point vibrational energy corrected values in parentheses.

Level of Theory	D_e (D_0) Triangular Li-ON	D_e (D_0) Linear Li-ON	D_e (D_0) Linear Li-NO
cc-pVTZ SCF	23.19 (22.76)	24.14 (23.63)	16.81 (15.57)
aug-cc-pVTZ SCF	23.61 (23.18)	24.47 (23.97)	17.39 (16.19)
cc-pCVTZ SCF	23.39 (22.96)	24.39 (23.88)	16.99 (15.75)
cc-pVQZ SCF	23.54 (23.10)	24.49 (23.96)	17.17 (15.94)
aug-cc-pVQZ SCF	23.55 (23.11)	24.43 (23.92)	17.29 (16.07)
cc-pCVQZ SCF	23.61 (23.16)	24.55 (24.02)	17.22 (15.99)
cc-pVTZ CISD	30.41 (29.71)	26.07 (25.38)	27.81 (26.51)
aug-cc-pVTZ CISD	31.50 (30.80)	27.26 (26.60)	29.26 (28.00)
cc-pCVTZ CISD	28.02 (27.30)	23.76 (23.04)	25.36 (24.03)
cc-pVQZ CISD	31.67 (30.95)	27.39 (26.69)	29.32 (28.05)
aug-cc-pVQZ CISD	32.00 (31.30)	27.76 (27.09)	29.81 (28.55)
cc-pCVQZ CISD	29.10 (28.36)	24.86 (24.13)	26.68 (25.36)
cc-pVTZ CCSD	33.86 (33.16)	28.08 (27.33)	30.99 (29.74)
aug-cc-pVTZ CCSD	35.01 (34.33)	29.56 (28.85)	32.60 (31.40)
cc-pCVTZ CCSD	34.61 (33.90)	28.79 (28.02)	31.64 (30.37)
cc-pVQZ CCSD	35.23 (34.52)	29.65 (28.90)	32.69 (31.45)
aug-cc-pVQZ CCSD	35.61 (34.79)	30.17 (29.44)	33.24 (32.02)
cc-pCVQZ CCSD	35.99 (35.26)	30.34 (29.56)	33.35 (32.08)
cc-pVTZ CCSD(T)	33.54 (32.79)	26.64 (25.83)	30.97 (29.69)
aug-cc-pVTZ CCSD(T)	34.88 (34.05)	28.48 (27.71)	32.92 (31.69)
cc-pCVTZ CCSD(T)	34.40 (33.63)	27.42 (26.60)	31.71 (30.41)
cc-pVQZ CCSD(T)	35.17 (34.41)	28.54 (27.74)	33.02 (31.76)
aug-cc-pVQZ CCSD(T)	35.59 (34.85)	29.17 (28.40)	33.67 (32.43)
cc-pCVQZ CCSD(T)	36.04 (35.27)	29.32 (28.49)	33.78 (32.49)

Table 3.9: Total energies (in hartree) for Li (^2S) and NO ($X\ ^2\Pi_{1/2}$).

Level of Theory	Li (^2S)	ON ($X\ ^2\Pi_{1/2}$)
cc-pVTZ SCF	-7.432 679	-129.292 158
aug-cc-pVTZ SCF		-129.293 780
cc-pCVTZ SCF	-7.432 679	
cc-pVQZ SCF	-7.432 695	-129.301 897
aug-cc-pVQZ SCF		-129.302 494
cc-pCVQZ SCF	-7.432 695	
cc-pVTZ CISD		-129.669 284
aug-cc-pVTZ CISD		-129.676 587
cc-pCVTZ CISD	-7.474 224	
cc-pVQZ CISD		-129.703 066
aug-cc-pVQZ CISD		-129.706 060
cc-pCVQZ CISD	-7.476 330	
cc-pVTZ CCSD		-129.697 891
aug-cc-pVTZ CCSD		-129.706 304
cc-pCVTZ CCSD	-7.474 226	
cc-pVQZ CCSD		-129.733 655
aug-cc-pVQZ CCSD		-129.736 995
cc-pCVQZ CCSD	-7.476 333	
cc-pVTZ CCSD(T)		-129.717 072
aug-cc-pVTZ CCSD(T)		-129.726 367
cc-pCVTZ CCSD(T)	-7.474 248	
cc-pVQZ CCSD(T)		-129.754 601
aug-cc-pVQZ CCSD(T)		-129.758 316
cc-pCVQZ CCSD(T)	-7.476 367	

cc-pVTZ SCF	1.608	1.261
aug-cc-pVTZ SCF	1.607	1.260
cc-pCVTZ SCF	1.605	1.261
cc-pVQZ SCF	1.603	1.259
aug-cc-pVQZ SCF	1.603	1.258
cc-pCVTZ SCF	1.602	1.259
cc-pVTZ CASSCF	1.630	1.302
aug-cc-pVTZ CASSCF	1.630	1.302
cc-pVQZ CASSCF	1.626	1.300
aug-cc-pVQZ CASSCF	1.627	1.300
cc-pVTZ CISD	1.626	1.265
aug-cc-pVTZ CISD	1.629	1.264
cc-pCVTZ CISD	1.613	1.265
cc-pVQZ CISD	1.621	1.260
aug-cc-pVQZ CISD	1.624	1.259
cc-pCVQZ CISD	1.609	1.259
cc-pVTZ CCSD	1.633	1.273
aug-cc-pVTZ CCSD	1.638	1.273
cc-pCVTZ CCSD	1.620	1.273
cc-pVQZ CCSD	1.629	1.268
aug-cc-pVQZ CCSD	1.632	1.268
cc-pCVQZ CCSD	1.616	1.268
cc-pVTZ CCSD(T)	1.637	1.279
aug-cc-pVTZ CCSD(T)	1.640	1.279
cc-pCVTZ CCSD(T)	1.624	1.279
cc-pVQZ CCSD(T)	1.635	1.274
aug-cc-pVQZ CCSD(T)	1.639	1.274
cc-pCVQZ CCSD(T)	1.620	1.274

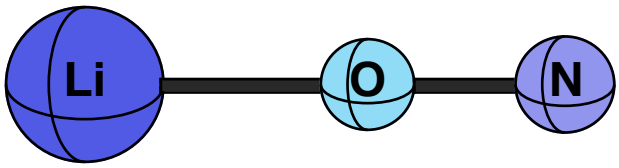

Figure 3.1: Predicted geometries for the $\tilde{X}\,^3\Sigma^-$ state of LiON at four levels of theoretical sophistication with four basis sets. Bond lengths are in Å.

cc-pVTZ SCF	1.714	1.183
aug-cc-pVTZ SCF	1.715	1.184
cc-pCVTZ SCF	1.712	1.183
cc-pVQZ SCF	1.712	1.182
aug-cc-pVQZ SCF	1.713	1.182
cc-pCVQZ SCF	1.712	1.182
cc-pVTZ CASSCF	1.724	1.235
aug-cc-pVTZ CASSCF	1.728	1.237
cc-pVQZ CASSCF	1.724	1.235
aug-cc-pVQZ CASSCF	1.726	1.235
cc-pVTZ CISD	1.717	1.203
aug-cc-pVTZ CISD	1.721	1.204
cc-pCVTZ CISD	1.706	1.202
cc-pVQZ CISD	1.715	1.200
aug-cc-pVQZ CISD	1.717	1.200
cc-pCVQZ CISD	1.703	1.198
cc-pVTZ CCSD	1.723	1.213
aug-cc-pVTZ CCSD	1.729	1.216
cc-pCVTZ CCSD	1.712	1.213
cc-pVQZ CCSD	1.723	1.211
aug-cc-pVQZ CCSD	1.725	1.212
cc-pCVQZ CCSD	1.709	1.210
cc-pVTZ CCSD(T)	1.726	1.221
aug-cc-pVTZ CCSD(T)	1.733	1.224
cc-pCVTZ CCSD(T)	1.714	1.221
cc-pVQZ CCSD(T)	1.726	1.219
aug-cc-pVQZ CCSD(T)	1.729	1.220
cc-pCVQZ CCSD(T)	1.712	1.218

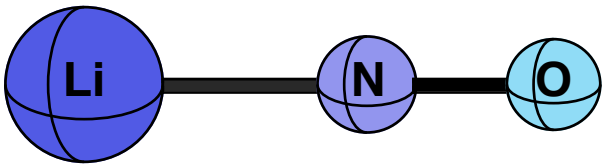

Figure 3.2: Predicted geometries for the $\tilde{X}\,^3\Sigma^-$ state of LiNO at four levels of theoretical sophistication with four basis sets. Bond lengths are in Å.

cc-pVTZ SCF	1.741	79.6	1.248	
aug-cc-pVTZ SCF	1.741	79.6	1.248	
cc-pCVTZ SCF	1.738	79.7	1.248	
cc-pVQZ SCF	1.736	79.7	1.247	
aug-cc-pVQZ SCF	1.737	79.7	1.246	
cc-pCVQZ SCF	1.735	79.7	1.247	
cc-pVTZ CASSCF	1.794		1.295	
aug-cc-pVTZ CASSCF	1.796		1.295	
cc-pVQZ CASSCF	1.789		1.293	
aug-cc-pVQZ CASSCF	1.790		1.293	
cc-pVTZ CISD	1.791		1.257	
aug-cc-pVTZ CISD	1.795		1.256	
cc-pCVTZ CISD	1.778		1.256	
cc-pVQZ CISD	1.785		1.252	
aug-cc-pVQZ CISD	1.788		1.251	
cc-pCVQZ CISD	1.771		1.250	
cc-pVTZ CCSD	1.802	75.0	1.271	
aug-cc-pVTZ CCSD	1.808	75.0	1.271	
cc-pCVTZ CCSD	1.789	75.1	1.272	
cc-pVQZ CCSD	1.798	75.1	1.266	
aug-cc-pVQZ CCSD	1.801		1.266	
cc-pCVQZ CCSD	1.782		1.266	
cc-pVTZ CCSD(T)	1.813	74.8	1.280	
aug-cc-pVTZ CCSD(T)	1.820	74.9	1.280	
cc-pCVTZ CCSD(T)	1.799	74.8	1.280	
cc-pVQZ CCSD(T)	1.809	74.9	1.275	
aug-cc-pVQZ CCSD(T)	1.813	75.0	1.275	
cc-pCVQZ CCSD(T)	1.793	74.9	1.275	
		74.1		
		74.2		
		74.0		
		74.3		
		74.4		
		74.1		
		73.4		
		73.5		
		73.3		
		73.5		
		73.6		
		73.4		

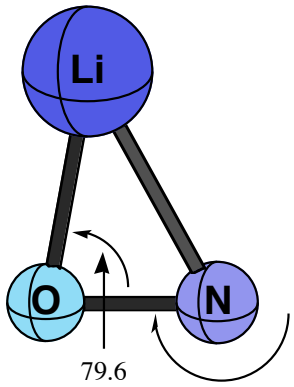

Figure 3.3: Predicted geometries for the $\tilde{X}\,^3A''$ state of LiON at four levels of theoretical sophistication with four basis sets. Bond lengths are in Å and angle in degrees.

cc-pVTZ SCF	1.682			111.1
aug-cc-pVTZ SCF	1.683			111.2
cc-pCVTZ SCF	1.680			111.0
cc-pVQZ SCF	1.678			111.1
aug-cc-pVQZ SCF	1.679			111.1
cc-pCVQZ SCF	1.677			111.1
cc-pVTZ CASSCF	1.693			123.4
aug-cc-pVTZ CASSCF	1.694			123.9
cc-pVQZ CASSCF	1.689			123.5
aug-cc-pVQZ CASSCF	1.690			123.8
cc-pVTZ CISD	1.682			124.2
aug-cc-pVTZ CISD	1.687			124.2
cc-pCVTZ CISD	1.672			123.5
cc-pVQZ CISD	1.679			124.1
aug-cc-pVQZ CISD	1.681			124.3
cc-pCVQZ CISD	1.667			123.5
cc-pVTZ CCSD	1.682			128.7
aug-cc-pVTZ CCSD	1.689			128.4
cc-pCVTZ CCSD	1.671			128.1
cc-pVQZ CCSD	1.680	1.268		128.3
aug-cc-pVQZ CCSD	1.683	1.267		128.4
cc-pCVQZ CCSD	1.667	1.268		127.7
		1.266		
cc-pVTZ CCSD(T)	1.683	1.265		130.6
aug-cc-pVTZ CCSD(T)	1.692	1.266		130.1
cc-pCVTZ CCSD(T)	1.671			130.0
cc-pVQZ CCSD(T)	1.682	1.311		130.1
aug-cc-pVQZ CCSD(T)	1.686	1.311		130.2
cc-pCVQZ CCSD(T)	1.668	1.309		129.5
		1.308		
		1.276		
		1.274		
		1.275		
		1.270		
		1.269		
		1.269		
		1.286		
		1.284		
		1.286		
		1.280		
		1.279		
		1.280		
		1.292		
		1.291		
		1.292		
		1.286		
		1.286		
		1.292		

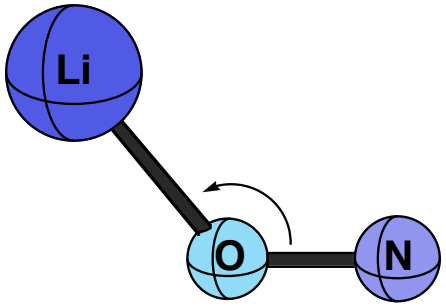

Figure 3.4: Predicted geometries for the $\tilde{X}\,^3A''$ transition state of LiON at four levels of theoretical sophistication with four basis sets. Bond lengths are in Å and angle in degrees.

cc-pVTZ SCF	114.2		1.792
aug-cc-pVTZ SCF	113.7		1.795
cc-pCVTZ SCF	114.0		1.791
cc-pVQZ SCF	113.6		1.792
aug-cc-pVQZ SCF	113.5		1.793
cc-pCVQZ SCF	113.6		1.791
cc-pVTZ CASSCF	125.0		1.798
aug-cc-pVTZ CASSCF	122.9		1.805
cc-pVQZ CASSCF	123.0		1.801
aug-cc-pVQZ CASSCF	122.5		1.804
cc-pVTZ CISD	112.3		1.793
aug-cc-pVTZ CISD	111.3		1.799
cc-pCVTZ CISD	112.0		1.783
cc-pVQZ CISD	111.3		1.793
aug-cc-pVQZ CISD	111.0		1.796
cc-pCVQZ CISD	111.2		1.781
cc-pVTZ CCSD	113.1		1.797
aug-cc-pVTZ CCSD	113.1		1.797
cc-pCVTZ CCSD	112.9		1.787
cc-pVQZ CCSD	111.9		1.798
aug-cc-pVQZ CCSD	111.6	1.207	1.802
cc-pCVQZ CCSD	111.8	1.208	1.785
		1.207	
cc-pVTZ CCSD(T)	113.4	1.206	1.799
aug-cc-pVTZ CCSD(T)	111.9	1.206	1.809
cc-pCVTZ CCSD(T)	113.2	1.206	1.788
cc-pVQZ CCSD(T)	112.1		1.801
aug-cc-pVQZ CCSD(T)	111.7	1.258	1.806
cc-pCVQZ CCSD(T)	112.0	1.260	1.787
		1.258	
		1.259	
		1.229	
		1.229	
		1.228	
		1.225	
		1.225	
		1.224	
		1.242	
		1.242	
		1.242	
		1.239	
		1.239	
		1.238	
		1.251	
		1.253	
		1.251	
		1.248	
		1.249	
		1.248	

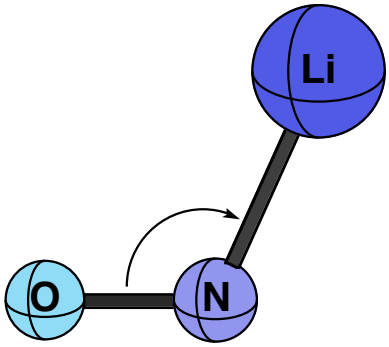

Figure 3.5: Predicted geometries for the $\tilde{X}\,^3A''$ transition state of LiNO at four levels of theoretical sophistication with four basis sets. Bond lengths are in Å and angle in degrees.

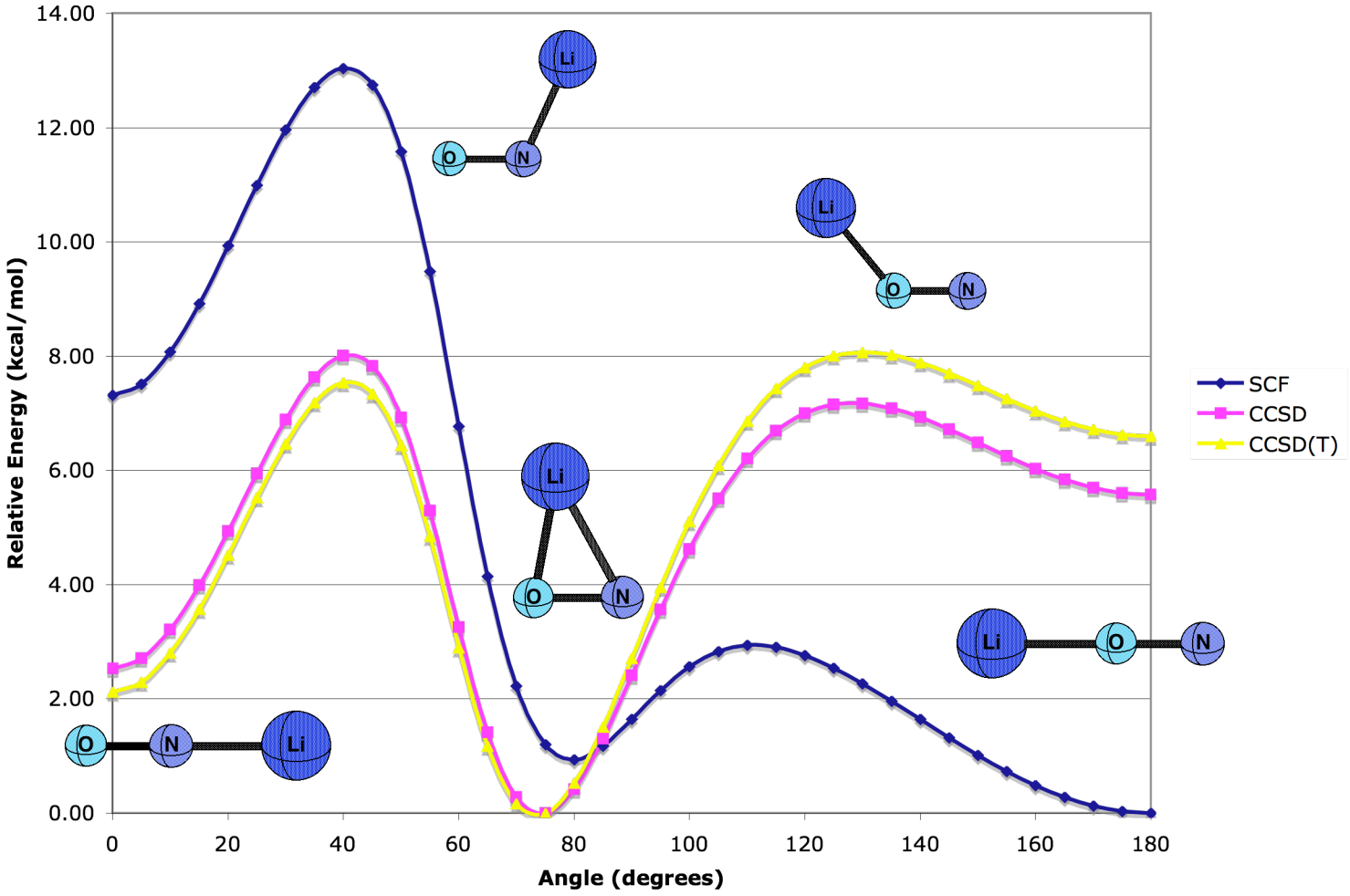

Figure 3.6: Diagrammatic potential energy surface of LiON at the cc-pVQZ CCSD(T) level of theory.

CHAPTER 4

CONCLUDING REMARKS

It is clear that the application of high levels of theory on small molecules is still of interest to both experimentalist and theorists. Indeed when inconsistencies arise a detailed analysis of why needs to be performed for the improvement of theory or experimental methods and a more complete understanding of the environment of the system. The need for understanding how these molecules behave provides invaluable information when looking at larger molecules.

Challenging problems related with the electronic structure of systems containing both metal-metal and metal-nonmetal bonding have been attempted with very sophisticated quantum mechanical *ab initio* methods such as coupled cluster theory up to and including full triples and multiconfigurational methods. Corrections due to the zero point vibrational energy and core-valence interactions (for lithium nitroxide) have been included, and large basis sets such as aug-cc-pVQZ have been employed.

For dialuminum monoxide it was found that the AlAlO isomer has only a barrier of 2.2 kcal mol^{-1} in going to the AlOAl global minimum and the AlOAl isomer has a barrier of 80.1 kcal mol^{-1} to the AlAlO. It is then not surprising that experimentalists have been unable to detect the AlAlO isomer. For lithium nitroxide the three possible lowest energy structures were studied. The best level of theory predicts that the bent isomer is the lowest with the LiNO and LiON isomer being 2.4 and 6.4 kcal mol^{-1} above, respectively. The LiNO isomer has a barrier of 4.5 kcal mol^{-1} to the bent isomer, whereas LiON only has a 0.9 kcal mol^{-1} barrier. The linear isomers themselves differ by 4.0 kcal mol^{-1} with the LiNO isomer being lower. These separations in relative energetics provide a distinction in the energy ordering of the three isomers when compared to previous theoretical studies.

In addition to the relative energies described above, physical and chemical properties such as bonding characteristics, equilibrium geometries, dipole moments, harmonic vibrational frequencies, and infrared intensities have been studied, and reliable values have been determined with the coupled cluster theories. Comparison with the available experimental data suggested that coupled cluster theory is able to predict bond distances within ±0.1 Å and energetic properties within ±1.0 kcal mol^{-1} accuracy when it is employed with large basis sets.

REFERENCES

[1] T. D. Crawford and H. F. Schaefer III, Rev. Comput. Chem. **14**, 33 (2000).

[2] I. N. Levine, *Quantum Chemistry*, 5th ed. (Prentice Hall, Englewood Cliffs, N. J., 2000).

[3] J. Paldus and X. Z. Li, Adv. Chem. Phys. **110**, 1 (1960).

[4] *Methods of Electronic Structure Theory*, edited by H. F. Schaefer III (Plenum Press, New York, 1977).

[5] C. D. Sherrill and H. F. Schaefer III, Adv. Quantum Chem. **34**, 143 (1999).

[6] A. Szabo and N. S. Ostlund, *Modern Quantum Chemistry: Introduction to Advanced Electronic Structure Theory*, 1st ed. (McGraw-Hill, New York, 1989).

[7] H.-J. Werner, Adv. Chem. Phys. **69**, 1 (1987).

[8] *Modern Electronic Structure Theory, Advanced Series in Physical Chemistry*, edited by D. R. Yarkony (World Scientific, Singapore, 1995).

[9] J. M. Foster and S. F. Boys, Rev. Mod. Phys. **32**, 300 (1960).

[10] M. Born and K. Huang, *Dynamical Theory of Crystal Lattices*. (Oxford University, New York, 1956).

[11] E. A. Hylleraas, Z. Phys. **54**, 347 (1929).

[12] E. A. Hylleraas, Z. Phys. **65**, 209 (1930).

[13] E. A. Hylleraas, Adv. Quantum Chem. **1**, 1 (1964).

[14] W. Kutzelnigg and W. Klopper, J. Chem. Phys. **94**, 1985 (1991).

[15] W. Kutzelnigg and J. D. Morgan, J. Chem. Phys. **96**, 4484 (1992).

[16] W. Kolos and L. Wolniewicz, J. Chem. Phys. **49** (404) (1968).

[17] P. O. Löwdin, Adv. Chem. Phys. **2**, 404 (1959).

[18] C. C. J. Roothaan, Rev. Mod. Phys. **23**, 69 (1951).

[19] P. Saxe, H. F. Schaefer III, and N. C. Handy, Chem. Phys. Lett. **79** (202) (1981).

[20] R. S. Mulliken, Phys. Rev. **32**, 168 (1928).

[21] J. C. Slater, Phys. Rev. **34**, 1293 (1929).

[22] J. C. Slater, Phys. Rev. **35**, 1930 (1930).

[23] C. C. J. Roothaan, Rev. Mod. Phys. **32**, 179 (1960).

[24] S. F. Boys, Proc. R. Soc. London, Ser. A **200**, 542 (1950).

[25] K. O-Ohata, H. Taketa, and S. Huzinaga, J. Phys. Soc. Jpn. **21**, 2306 (1966).

[26] I. Shavitt, in *Applications of Electronic Structure Theory*, edited by H. F. Schaefer III (Plenum, New York, 1977), Vol. 3.

[27] O. Sinanoglu, J. Chem. Phys. **36**, 706 (1962).

[28] A. C. Wahl, J. Chem. Phys. **41**, 2600 (1964).

[29] J. Čížek, J. Chem. Phys. **45**, 4256 (1966).

[30] J. Čížek, Adv. Chem. Phys. **14**, 35 (1969).

[31] J. Čížek and J. Paldus, Int. J. Quantum Chem. **5**, 359 (1971).

[32] A. C. Hurley, *Electron Correlation in Small Molecules*. (Academic Press, London, 1976).

[33] J. A. Pople, R. Krishman, H. B. Schlegel, and J. S. Binkley, Int. J. Quantum Chem. **14**, 545 (1978).

[34] R. J. Bartlett and G. D. Purvis, Int. J. Quantum Chem. **14**, 561 (1978).

[35] G. D. Purvis and R. J. Bartlett, J. Chem. Phys. **98**, 1358 (1982).

[36] T. J. Lee and J. E. Rice, Chem. Phys. Lett. **150**, 406 (1988).

[37] G. D. Purvis and R. J. Bartlett, J. Chem. Phys. **75**, 1284 (1981).

[38] G. E. Scuseria, C. L. Janssen, and H. F. Schaefer III, J. Chem. Phys. **89**, 7382 (1988).

[39] G. E. Scuseria, T. J. Lee, and H. F. Schaefer III, Chem. Phys. Lett. **130**, 236 (1986).

[40] G. E. Scuseria, A. C. Scheiner, T. J. Lee, J. E. Rice, and H. F. Schaefer III, J. Chem. Phys. **86**, 2881 (1987).

[41] J. F. Stanton, J. Gauss, J. D. Watts, and R. J. Bartlett, J. Chem. Phys. **94**, 4334 (1991).

[42] M. J. O. Deegan and P. J. Knowles, Chem. Phys. Lett. **227**, 321 (1994).

[43] M. R. Hoffman and H. F. Schaefer III, Adv. Quantum Chem. **18**, 207 (1986).

[44] S. A. Kucharski and R. J. Bartlett, J. Chem. Phys. **97**, 4282 (1992).

[45] Y. S. Lee, S. A. Kucharski, and R. J. Bartlett, J. Chem. Phys. **81**, 5906 (1984).

[46] J. Noga, R. J. Bartlett, and M. Urban, Chem. Phys. Lett. **134**, 126 (1987).

[47] G. E. Scuseria and H. F. Schaefer III, Chem. Phys. Lett. **152**, 382 (1988).

[48] M. Urban, J. Noga, S. J. Cole, and R. J. Bartlett, J. Chem. Phys. **83**, 4041 (1985).

[49] L. Adamowicz, W. D. Laidig, and R. J. Bartlett, Int. J. Quantum Chem. **18**, 245 (1984).

[50] G. B. Fitzgerald, R. J. Harrison, W. D. Laidig, and R. J. Bartlett, Chem. Phys. Lett. **117**, 433 (1985).

[51] P. Jørgensen and J. Simons, J. Chem. Phys. **79**, 1983 (1983).

[52] A. C. Scheiner, G. E. Scuseria, J. E. Rice, T. J. Lee, and H. F. Schaefer III, J. Chem. Phys. **87**, 5361 (1987).

[53] G. E. Scuseria, J. Chem. Phys. **94**, 442 (1991).

[54] J. Gauss and J. F. Stanton, Chem. Phys. Lett. **276**, 70 (1997).

[55] H. Koch, H. J. A. Jensen, P. Jørgensen, T. Helgaker, G. E. Scuseria, and H. F. Schaefer III, J. Chem. Phys. **92**, 4924 (1990).

[56] E. A. Salter and R. J. Bartlett, J. Chem. Phys. **90**, 1989 (1989).

[57] J. Noga and R. J. Bartlett, J. Chem. Phys. **86**, 7041 (1987).

[58] J. D. Watts and R. J. Bartlett, J. Chem. Phys. **93**, 6104 (1990).

[59] H. Koch, O. Christiansen, P. Jørgensen, A. M. S. de Maras, and T. Helgaker, J. Chem. Phys. **106**, 1808 (1997).

[60] A. C. Wahl and G. Das, in *Methods of Electronic Structure Theory*, edited by H. F. Schaefer III (Plenum Press, New York and London, 1977), Vol. 3, pp. 51.

[61] K. P. Huber and G. Herzberg, *Constants of Diatomic Molecules*. (Van Nostrand Reinhold, New York, 1979).

[62] G. Drowart, G. DeMaria, R. P. Burns, and M. G. Inghram, J. Chem. Phys. **32**, 1366 (1960).

[63] A. Buchler, J. L. Stauffer, W. Klemperer, and L. Wharton, J. Chem. Phys. **39**, 2299 (1963).

[64] M. J. Linevsky, D. White, and D. E. Mann, J. Chem. Phys. **41**, 542 (1964).

[65] A. Snelson, J. Chem. Phys. **74**, 2574 (1970).

[66] D. M. Makowiecki, D. A. Lynch, and K. D. Carlson, J. Phys. Chem. **75**, 1963 (1971).

[67] C. P. Marino and D. White, J. Phys. Chem. **77**, 2929 (1973).

[68] D. A. Lynch, M. J. Zehe, and K. D. Carlson, J. Phys. Chem. **78**, 236 (1974).

[69] M. A. Douglas, R. H. Hauge, and J. L. Margrave, High. Temp. Sci. **16**, 35 (1982).

[70] L. Andrews, T. R. Burkholder, and J. T. Yustein, J. Phys. Chem. **96**, 10182 (1992).

[71] M. Cai, C. C. Carter, T. A. Miller, and V. E. Bondybey, J. Chem. Phys. **95**, 73 (1991).

[72] S. M. Sonchik, L. Andrews, and K. D. Carlson, J. Phys. Chem. **87**, 2004 (1983).

[73] I. V. Ovchinnikov, L. V. Serebrennikov, and A. A. Mal'tsev, Russ. J. Phys. Chem. **59**, 923 (1985).

[74] I. L. Rozhanskii, L. V. Serebrennikov, and A. F. Shevel'kov, Russ. J. Phys. Chem. **64**, 276 (1990).

[75] E. L. Wagner, Theor. Chim. Acta **32**, 295 (1974).

[76] L. P. Davis, R. M. Guiidry, J. R. Williams, M. J. S. Dewar, and H. S. Rzepa, J. Comput. Chem. **2**, 433 (1981).

[77] R. D. Srivastava and M. Farber, Chem. Rev. **78**, 627 (1978).

[78] L. Pauling, *The Nature of the Chemical Bond*. (Cornell University Press, Ithaca, N.Y., 1960).

[79] J. Masip, A. Clotet, J. M. Ricart, F. Illas, and J. Rubio, Chem. Phys. Lett. **144**, 373 (1988).

[80] A. I. Boldyrev and P. V. R. Schleyer, J. Am. Chem. Soc. **113**, 9045 (1991).

[81] A. V. Nemukhim and F. Weinhold, J. Chem. Phys. **97**, 3420 (1992).

[82] J. Koput and A. Gertych, J. Chem. Phys. **121**, 130 (2004).

[83] T. H. Dunning, J. Chem. Phys. **90**, 1007 (1989).

[84] T. H. Dunning, K. A. Peterson, and A. K. Wilson, J. Chem. Phys. **114**, 9244 (2001).

[85] D. E. Woon and T. H. Dunning, J. Chem. Phys. **98**, 1358 (1993).

[86] M. Yoshimine, A. D. McLean, and B. Liu, J. Chem. Phys. **58**, 4412 (1973).

[87] C. Zenouda, P. Blottiau, G. Chambaud, and P. Rosmus, J. Mol. Struct. **458**, 61 (1999).

[88] G. L. Gutsev, R. Jena, and R. J. Bartlett, J. Chem. Phys. **110**, 2928 (1999).

[89] M. Rittby and R. J. Bartlett, J. Phys. Chem. **92**, 3033 (1988).

[90] K. Raghavachari, G. W. Trucks, J. A. Pople, and M. Head-Gordon, Chem. Phys. Lett. **157**, 479 (1989).

[91] G. E. Scuseria, Chem. Phys. Lett. **176**, 27 (1991).

[92] C. L. Janssen, E. T. Seidl, G. E. Scuseria, T. P. Hamilton, Y. Yamaguchi, R. B. Remington, Y. Xie, G. Vacek, C. D. Sherrill, T. D. Crawford, J. T. Fermann, W. D. Allen, B. R. Brooks, G. B. Fitzgerald, D. J. Fox, J. F. Gaw, N. C. Handy, W. D. Laidig, T. J. Lee, R. M. Pitzer, J. E. Rice, P. Saxe, A. C. Scheiner, and H. F. Schaefer III, PSI2 (PSITECH, Inc., Watkinsville, GA 30677, 1995).

[93] T. D. Crawford, C. D. Sherrill, E. F. Valeev, J. T. Fermann, R. A. King, M. L. Leininger, S. T. Brown, C. L. Janssen, E. T. Seidl, J. P. Kenny, and W. D. Allen, PSI3.2 (2003).

[94] J. F. Stanton, J. Gauss, W. J. Lauderdale, J. D. Watts, and R. J. Bartlett, ACESII: The package also contains modified versions of the MOLECULE Gaussian integral program of J. Almlöf and P. R. Taylor, the ABACUS integral derivative program written by T. U. Halgaker, H. J. A. Jensen, P. Jørgensen, and P. R. Taylor, and the PROPS property evaluation integral code of P. R. Taylor.

[95] P. J. Knowles and H.-J. Werner, Chem. Phys. Lett. **115**, 259 (1985).

[96] P. J. Knowles and H.-J. Werner, Chem. Phys. Lett. **145**, 514 (1988).

[97] H.-J. Werner and P. J. Knowles, J. Chem. Phys. **82**, 5053 (1985).

[98] H.-J. Werner and P. J. Knowles, J. Chem. Phys. **89**, 5803 (1988).

[99] H.-J. Werner and W. Meyer, J. Chem. Phys. **74**, 5794 (1981).

[100] T. P. Straatsma, E. Apra, T. L. Windus, E. J. Bylaska, W. de Jong, S. Hirata, M. Valiev, M. Hackler, L. Pollack, R. J. Harrison, M. Dupuis, D. M. A. Smith, J. Nieplocha, V. Tipparaju, M. Krishnan, A. A. Auer, E. Brown, G. Cisneros, G. Fann, H. Fruchtl, J. Garza, K. Hirao, R. A. Kendall, J. Nichols, K. Tsemekhman, K. Wolinski, J. Anchell, D. Bernholdt, P. Borowski, T. Clark, D. Clerv, H. Dachsel, M. Deegan, K. Dyall, D. Elwood, E. Glendening, M. Gutowski, A. Hess, J. Jaffe, B. Jognson, J. Ju, R. Kobayashi, R. Kutteh, Z. Lin, R. Littlefield, X. Long, B. Meng, T. Nakajima, S. Niu, M. Rosing, G. Sandrone, M. Stave, H. Taylor, G. Thomas, J. van Lenthe, A. Wong, and Z. Zhang, NWCHEM, A Computational Chemistry Package for Parallel Computers, Version 4.6 (Pacific Northwest National Laboratory, Richland, Washington 99352-0999, USA, 2004).

[101] G. S. Hammond, J. Am. Chem. Soc. **77**, 334 (1955).

[102] R. M. Badger, J. Chem. Phys. **2**, 128 (1934).

[103] R. M. Badger, J. Chem. Phys. **3**, 710 (1935).

[104] M. W. Chase, C. A. Davies, J. R. Downey, D. J. Frurip, R. A. McDonald, and A. N. Syverund, *NIST-JANAF Thermochemical Tables*, 4 ed. (American Chemical Society and American Institute of Physics, New York, 1998).

[105] M. Farber, R. D. Srivastava, and O. M. Uy, J. Chem. Soc., Faraday Trans. **68**, 249 (1972).

[106] R. W. Asmussen, Acta. Chem. Scand. **11**, 1435 (1957).

[107] L. Andrews and G. C. Pimentel, J. Chem. Phys. **44**, 2361 (1966).

[108] J. Peslak, D. S. Klett, and C. W. David, J. Am. Chem. Soc. **93**, 5001 (1970).

[109] D. E. Tevault and L. Andrews, J. Chem. Phys. **77**, 1640 (1973).

[110] N. Girard-Dussau, A. Dargelos, and M. Chaillet, J. Mol. Struct. **89**, 123 (1982).

[111] M. Spoliti, F. Ramondo, F. Diomedi-Camassei, and L. Bencivenni, J. Mol. Struct. **312**, 41 (1994).

[112] E. Vayner and D. W. Ball, J. Mol. Struct. **542**, 149 (2001).

[113] R. D. Amos, A. Bernhardsson, A. Berning, P. Celani, D. L. Cooper, M. J. O. Deegan, A. J. Dobbyn, F. Eckert, C. Hampel, G. Hetzer, P. J. Knowles, T. Korona, R. Lindh, A. W. Lloyd, S. J. McNicholas, F. R. Manby, W. Meyer, M. E. Mura, A. Nickass, P. Palmieri, R. M. Pitzer, G. Rauhut, U. Schütz, U. Schumann, H. Stoll, A. J. Stone, R. Tarroni, T. Thorsteinsson, and H.-J. Werner, MOLPRO, a package of *ab initio* programs designed by H.-J. Werner and P. J. Knowles, version 2002.1.

[114] L. Andrews, M. Zhou, and X. Wang, J. Phys. Chem. A **104**, 8475 (2000).

[115] R. M. Neumann, Astrophys. J. **161**, 779 (1970).

[116] L. Andrews and B. Liang, J. Am. Chem. Soc. **123**, 1997 (2000).